AD-A273 905

VIBRATIONAL ENERGY TRANSFER WITHIN THE $B^3\Pi(O_u^+)$ STATE OF $^{79}Br_2$ UPON COLLISION WITH N_2, O_2, NO, AND SF_6

THESIS

Gregory S. Williams

Captain, USAF

AFIT/GAP/ENP/93D-10

93-30512

93 12 15 128

VIBRATIONAL ENERGY TRANSFER WITHIN THE $B^3\Pi(O_u^+)$ STATE OF $^{79}Br_2$ UPON COLLISION WITH N_2, O_2, NO, AND SF_6

THESIS

Presented to the Faculty of the Graduate School of Engineering

of the Air Force Institute of Technology

Air University

In Partial Fulfillment of the

Requirements for the Degree of

Master of Science in Engineering Physics

Gregory S. Williams, B.S.

Captain, USAF

December 1993

Accesion For		
NTIS CRA&I		☒
DTIC TAB		☐
Unannounced		☐
Justification		
By		
Distribution /		
Availability Codes		
Dist	Avail and / or Special	
A-1		

Approved for public release; distribution unlimited

Preface

This research has been but a small part of an overall effort at AFIT to determine the vibrational transfer rates and electronic quenching rates of the diatomic interhalogens in determining potential candidates for visible chemical lasers. This thesis is a continuation of a study started by Capt. Courtney Holmberg in his doctoral research to test the validity of the various energy transfer models in $Br_2(B)$. The objective is to further characterize vibrational energy transfer in $Br_2(B)$ with molecular collision partners using pulsed, laser induced fluorescence techniques.

Many individuals have helped in the completion of this research. I am profoundly grateful to my thesis advisor, Maj. Glen Perram, who has given a lot of his time, effort, and encouragement since my arrival at AFIT. I am also deeply indebted to Capt. Courtney Holmberg who spent much of his time helping to reinstall the experimental apparatus and ensuring that I had the knowledge to operate it. Thanks go to Mr. Jim Reynolds and Mr. Greg Smith for their assistance throughout this project. I also want to thank my classmates for their support and friendship throughout the program at AFIT.

Finally, I want to thank my best friend and wife, Margie, for her continued love, understanding, and encouragement. She was the key to successfully completing AFIT, and is the key to succeeding in life.

<div align="right">Gregory S. Williams</div>

Table of Contents

List of Figures

List of Tables

Abstract

Vibrational transfer and electronic quenching in the lower vibrational levels of the $^{79}Br_2$(B; v' $\leq$ 3) were investigated using spectrally resolved, temporally resolved pulsed laser induced fluorescence techniques. Spectrally resolved emissions from collisionally populated Br_2(B) vibrational levels were observed for N_2, O_2, NO, and SF_6 collision partners. The vibrational transfer was efficient in the nonpredissociatve vibrational levels and is adequately described by the Montroll-Shuler model. An average fundamental vibrational transfer rate coefficient of k_v(1,0) = 3.4 ($\pm$0.6)x 10^{-11} cm^3/molec-sec predicts the vibrational transfer rates for the 0 $\leq$ v' $\leq$ 3 collisions with N_2, and a rate of k_v(1,0) = 2.9 ($\pm$0.6) x 10^{-11} cm^3/molec-sec for collisions with O_2. Vibrational rates for NO and SF_6 range from 1.5 ($\pm$0.2) x 10^{-11} cm^3/molec-sec to 4.0 ($\pm$1.1) x 10^{-11} cm^3/molec-sec. Electronic quenching rates for the observed vibrational levels were determined from the same data. Quenching rates were seen to be vibrationally dependent and went from a low of k_q = 0.4 ($\pm$0.1)x10^{-11} cm^3molec-sec for N_2 (pump v'=2 , view v'=1) to a high of k_q = 6.9 ($\pm$1.1) x 10^{-11} cm^3/molec-sec for NO (pump v'=3, view v'=2).

Vibrational Energy Transfer Within the $B^3\Pi(O_u^+)$ State of $^{79}Br_2$ Upon Collision With N_2, O_2, NO, and SF_6

I. Introduction

1.1 Overview

Much study has been performed on the spectroscopy and kinetics of the diatomic halogens and interhalogens because of their favorable characteristics as lasant species for visible chemical lasers. These characteristics include maintaining a population inversion, having long radiative lifetimes, and having relatively low quenching rates.[10] Iodine monofluoride (IF), bromine monochloride (BrCl), and bromine monofluoride (BrF) have been studied extensively for their potential as chemical lasers.[17,12,10,16,14] The recent study of vibrational energy transfer of $Br_2(B)$ with $Br_2(X)$ and the rare gases has been completed by Holmberg.[8] Br_2 is not a good candidate as a lasant species because of high loss due to predissociation; however, it is of scientific interest to extend Holmberg's work and study the vibrational energy transfer rates of $Br_2(B)$ with N_2, O_2, NO, and SF_6. These rates are compared with the rates from the theoretical models that are used to describe them.

1.2 Halogens and Interhalogens

One of the properties of the diatomic halogens that has made them strong candidates for visible, chemical lasers is that the internuclear spacing of the excited B-state is larger than in the ground X-state. The Franck-

Condon principle states that any transition will be vertical.[5] Thus, any B→X transition from low-lying vibrational levels of the excited electronic state (v') will terminate on sparsely populated, higher-lying vibrational levels of the ground electronic state (v"), virtually guaranteeing a population inversion. Also, the low electronic quenching rates (10^{-14}-10^{-10} cm^3/molec-sec) and relatively long radiative lifetimes (0.2-80 microsec) of the halogens and interhalogens are important factors for lasing.[4]

Unlike an optically pumped B→X laser, a chemical laser will probably excite the upper state across a range of B-state vibrational levels. To be a good lasant species, these energy levels should quickly thermalize through vibrational transfer to a lower level where lasing can proceed from v' = 0. Likewise, the vibrational transfer within the B-state should be quicker than the non-radiative loses due to both electronic quenching, which is the collisional deactivation of electronically excited molecules, and predissociation, where the excited molecule separates to atomic products.

1.3 Bromine

Bromine has been found to have a large loss of its energy due to a strong predissociation in vibrational levels above v' ≥ 4 in the $Br_2(B)$ state. Therefore, it is not considered to be a good lasant molecule, although Perram and Davis have made an optically pumped Br_2 laser.[13] Another loss mechanism in bromine is quenching. Clyne and coworkers reported that the effective electronic quenching rate for v' = 2 is around ten times smaller than of those reported for v' ≥ 4. [1] Because of this, Holmberg [8] conducted

vibrational transfer experiments of $Br_2(B)$ with $Br_2(X)$ and the rare gases below $v' \leq 4$.

1.4 Problem Statement

Pulsed LIF techniques were used to investigate the collisional energy transfer within the non-predissociative lower lying levels ($v' = 1-3$) of $Br_2(B)$ in the presence of diatomic and polyatomic molecules. Specific states were excited by a narrow linewidth pulsed dye laser, and emissions from specific vibrational levels were spectrally resolved with a monochromator. As the excited Br_2 deactivated to lower vibrational levels, the time profile indicated the rate of vibrational transfer as well as the rate of quenching. These rates were then used to test the validity of existing vibrational transfer theories.

These results were compared to Holmberg's work that analyzed the vibrational energy transfer of $Br_2(B)$ with $Br_2(X)$ and the rare gases. The results were also compared to other similar studies in halogens and interhalogens.

1.5 Organization

Chapter II will present a review of halogen molecular theory, laser induced fluorescence techniques, kinetic energy transfer, and vibrational energy transfer in the lower v' states in $Br_2(B)$. Chapter III will discuss the experimental apparatus and procedures used. Chapter IV will present the data obtained from the experimental runs as well as discuss the results. Chapter V will present the overall conclusions of this thesis with recommendations for future study.

II. Background Theory

2.1 Halogen and Interhalogen Structure

The halogen atoms, F, Cl, Br, I, and At all have a ground state outer electron shell configurations of $s^2 p^5$ that results in the spin-orbit term symbols of $^2P_{3/2}$ and $^2P_{1/2}$. Ground state diatomic halogens and interhalogens have a molecular orbital outer shell configuration of $(\sigma_g)^2 (\pi_u)^4 (\pi_g)^4 (\sigma_u)^0$ or (2440), and that state is designated $X^1\Sigma_g^+$ (see Figure 1). Excited states occur when one of these electrons is excited to the empty σ_u level. The $B^3\Pi(0_u^+)$ state is one of these excited states that correlates to the 2431 configuration. This study concentrates on the vib͟ ͟tional transfer rates within this excited state.
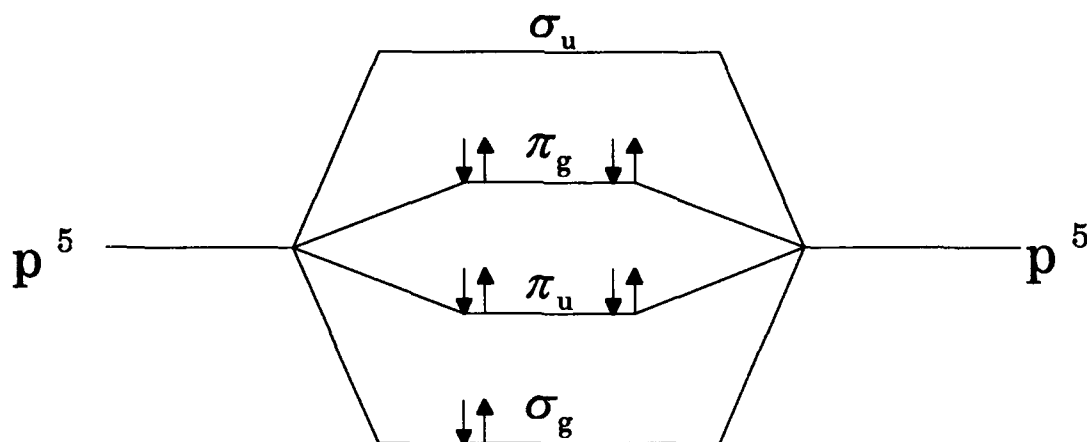
Figure 1. Ground state diatomic halogen electronic configuration.

2.2 Predissociation

Predissociation results when bound electronic state vibrational energy levels overlap with continuum energy levels from another electronic state, resulting in a radiationless transition from an excited molecular state into separated atoms. The predissociation in $Br_2(B)$ was determined by Clyne, Heaven, and Tellinghuisen [2] to be caused by a crossing of the $^3\Pi(0_u^+)$ curve by a $^1\Pi_u$ repulsive state between v' = 4 and v' = 5 as shown in Figure 2. Therefore, vibrational levels v' $\leq$ 3 are relatively unaffected by predissociation.
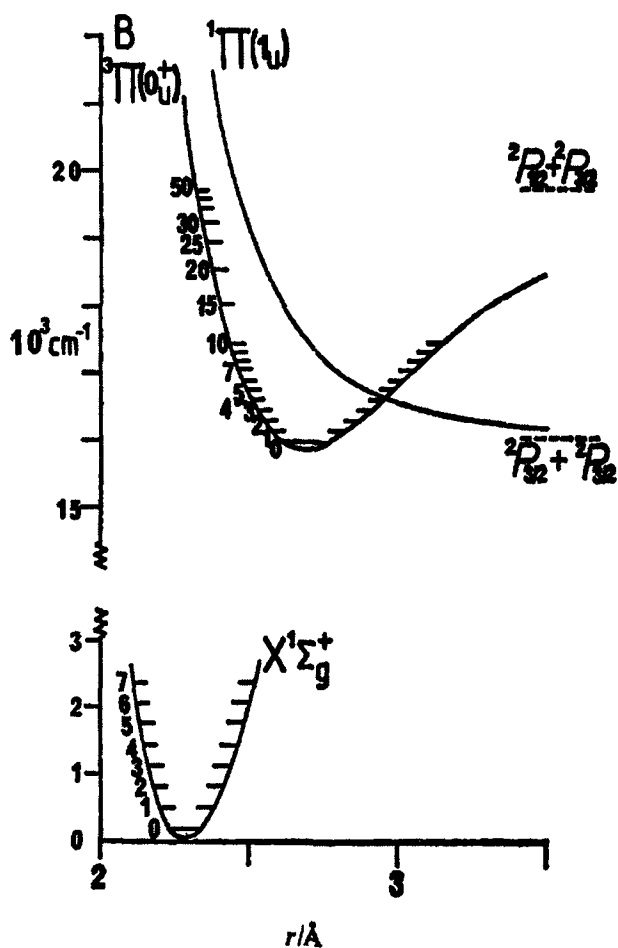
Figure 2. Br_2 potential energy curves. [1]

2.3 Laser Induced Fluorescence

Laser induced fluorescence (LIF) consists of using a tunable, narrow linewidth pulsed or cw laser to selectively excite an atom or molecule to a specific rovibrational quantum level in an excited electronic state and observing the resulting fluorescence as the excited atom or molecule relaxes back to the ground state. This fluorescence can come from either the "parent" state or a collisionally populated "satellite" state. An example of this is shown in Figure 3 where a laser is tuned to excite the parent state V. Satellite states, V-1 and V+1, are populated by collisional energy transfer. Eventually, the excited states decay back to ground states through either radiative or collisional processes. By using a monochromator to detect a specific excited state and also observing its time profile, collisional transfer rates can be derived. Examples of pulsed LIF techniques on parent and satellite states are seen in Figure 4.

The fluorescence intensity is directly proportional to the population of the excited state, and this can be used in CW LIF to find collisional energy transfer rates when analyzed with time-independent techniques. In the present experiment, only pulsed excitation is used, and the time profile is the critical analytical tool. The intensity of the fluorescence is mainly needed for a good signal-to-noise ratio.
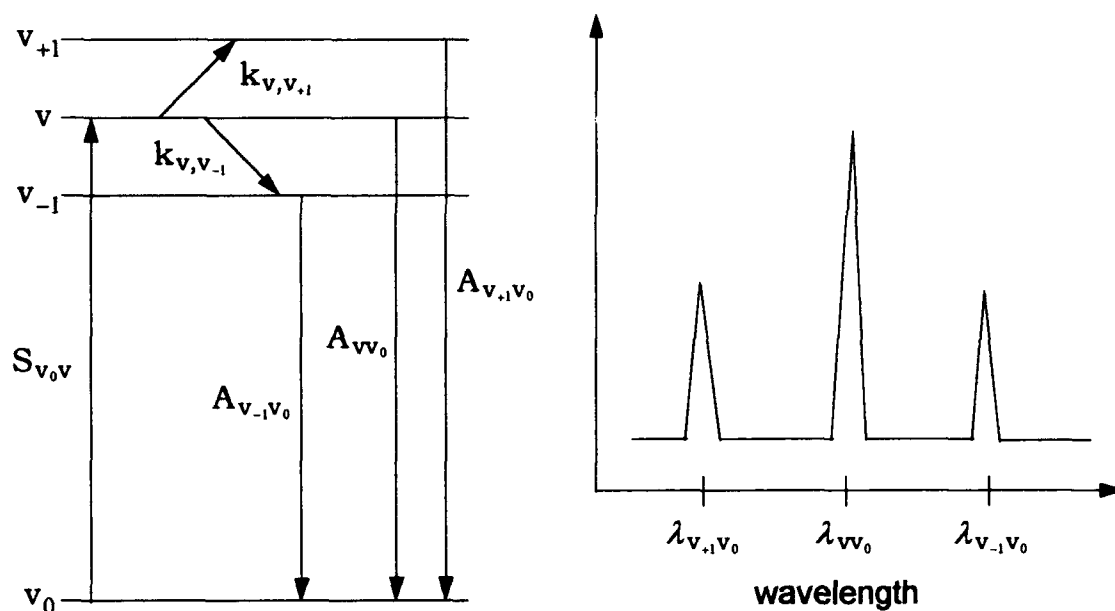
Figure 3. Simplified representation of laser induced fluorescence from
collisionally populated satellite states.[8]
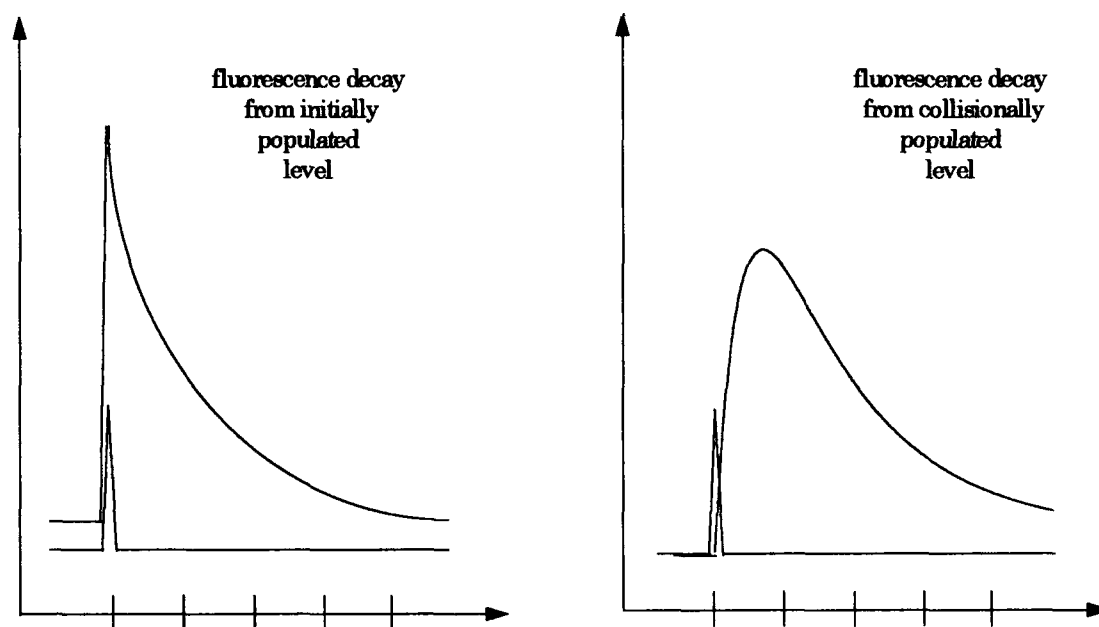
Figure 4.   Example of pulsed laser induced fluorescence technique from
parent and collisionally populated satellite states.[8]

2.4 Kinetic Analysis

The goal of this experiment was to investigate the collisional energy transfer processes within the non-predissociative vibrational levels $(0 \leq v' \leq 4)$ of the $Br_2 B^3\Pi(0_u^+)$ electronic state when combined with other diatomic or polyatomic species. To understand the relevant kinetic processes of the LIF experiment, a brief description of the energy transfer mechanisms is presented as well as the development of the master rate equation. Solutions to the master rate equation and discussion of the energy transfer theories follow.

2.4.1 Energy Transfer

The collisional, non-collisional, and radiative energy transfer processes that apply to all vibrational levels of the $Br_2 B^3\Pi(0_u^+)$ state are pictured in Figure 5 and are described mathematically as follows:

Optical excitation;

$$Br_2(X;v''_o) + h\upsilon_{pump} \xrightarrow{\ k_p\ } Br_2(B;v'_o) \tag{1}$$

Spontaneous emission;

$$Br_2(B;v'_o) \xrightarrow{\ A\ } Br_2(X;v'') + h\upsilon_{emission} \tag{2}$$

Predissociation;

$$Br_2(B;v'_o) \xrightarrow{\ \Gamma_{pd}\ } Br\left(^2P_{3/2}\right) + Br\left(^2P_{3/2}\right) \tag{3}$$

Electronic quenching;

$$Br_2(B;v') + Y \xrightarrow{\ k_{eq}\ } Br_2(X,A,A',...) + Y^* \tag{4}$$
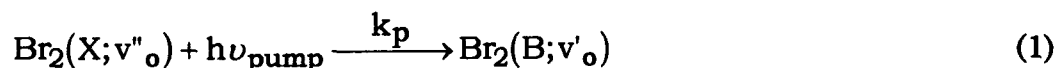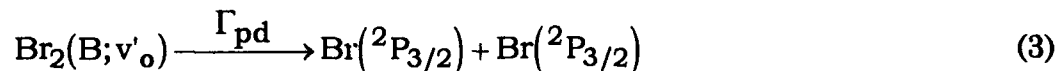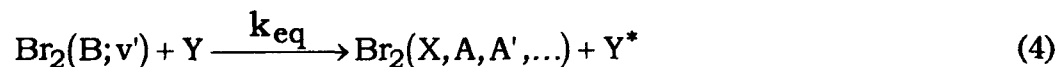
Rovibrational transfer (V,R→T);

$$Br_2(B;v',J') + Y \xrightarrow{\quad k_{VT} \quad} Br_2(B;v'+\Delta v',J'+\Delta J') + Y^*$$ (5)
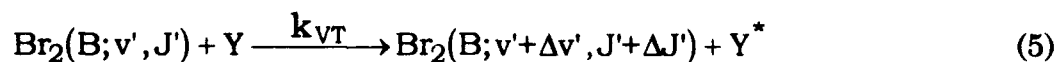
Vibrational-Vibrational Transfer (V→V);

$$Br_2(B;v') + Y(w) \xrightarrow{\quad k_{VV} \quad} Br_2(B;v'+\Delta v') + Y(w + \Delta w)$$ (6)
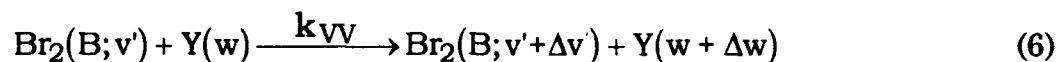
In the preceding equations, "Y" denotes an arbitrary atomic or molecular collision partner.
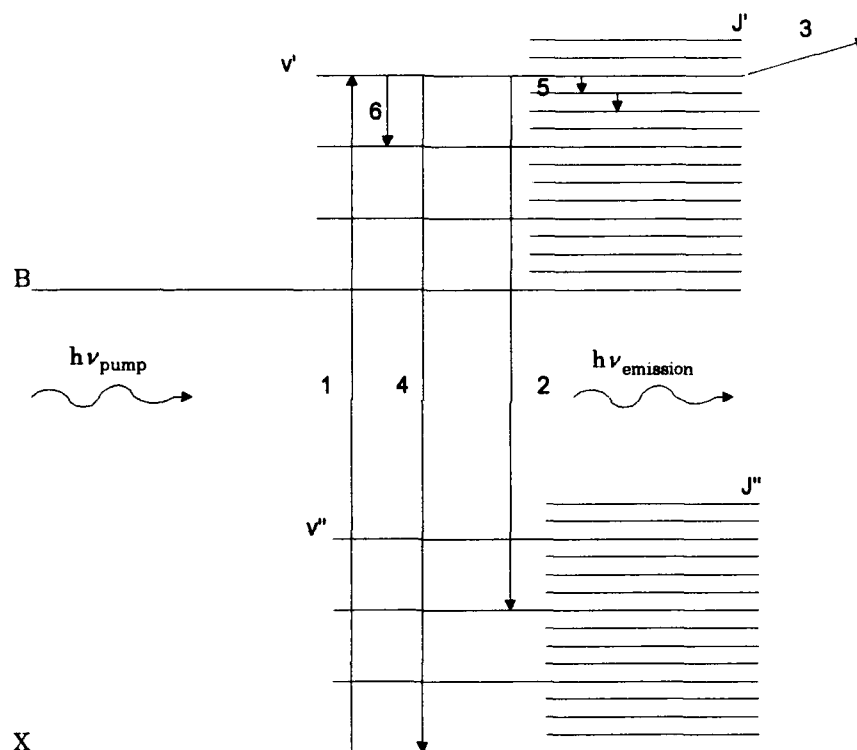
Figure 5. Energy transfer process.[10]

Optical excitation, Eq (1), and represented by transition (1) in Figure 5, is the method by which the laser excites the ground state molecule into an electronically excited B-state. The parent state is the specific $Br_2(B;v'_o)$ that

is initially populated. To populate this state exclusively, the pump laser linewidth must be smaller than the absorption laser linewidth.

Spontaneous emission, Eq (2) and transition (2), is the radiative decay of the excited state and the diagnostic tool of LIF. The radiative lifetime from state v' is proportional to the sum of Einstein A coefficients from v' to all v''

$$1/\tau_r(v') = A(v') = \sum_{v'',J''} A(v',J' \to v'',J'') \tag{7}$$

Predissociation, Eq (3) and transition (3), is a nonradiative loss process that can occur either spontaneously or collisionally. For example, a collision of $Br_2(B,v' = 4)$ with molecule Y can increase its energy to level v' = 5 where it spontaneously predissociates. The collisionless lifetime of the excited state is a combination of the radiative lifetime and predissociation as in Eq (8).

$$\Gamma_0(v') = 1/\tau_0(v') = 1/\tau_r(v') + \Gamma_{pd} \tag{8}$$

Since the experiments were conducted below the predissociative crossing, the pre-dissociation mechanisms were minimized.

The rest of the energy transfer mechanisms also involve nonradiative loss processes, but all occur collisionally. Electronic quenching, Eq (4) and transition (4), occurs when a collision with another molecule sends the $Br_2(B)$ molecule to any lower electronic state.

Rovibrational energy transfer, Eq (5) and transitions (5) and (6), is the transfer of either rotational or vibrational energy to the kinetic energy of the bath gas particle Y. The transfer is purely rotational or purely vibrational if $\Delta v = 0$ or $\Delta J = 0$, respectively. The rotational transfer rate is not observed in the lower v' levels for these experiments.

Vibrational-vibrational (V-V) transfer, Eq (6) and also represented by transition (6), occurs with molecular buffer gases. Both V-V and V-T transfer

are the mechanisms responsible for thermalization in $Br_2(B)$. The total vibrational transfer rate for this experiment is the sum of these two rates

$$k_V = k_{VT} + k_{VV} \tag{9}$$

If V-V transfer from the molecular buffer gases is considerable, then an increase in the total vibrational transfer rates is also expected.

The equations above describe state to state transitions for a single collision partner. Eq (10) describes the total vibrational transfer rate out of a single vibrational state to all other vibrational levels for collision partner Y.

$$K_V^Y(v) = \sum_{\Delta v} k_V^Y(v \rightarrow v + \Delta v) \tag{10}$$

2.4.2 Master Rate Equation

Following a derivation by Perram,[12] the terms described above are combined to create a master rate equation, Eq (11), that describes the population rate in a non-predissociative vibrational state (B;v).

$$\begin{aligned}
dN(B;v)/dt = {} & S\delta_{vv_o} - \Gamma_o(v) \, N(B;v) \\
& -\sum_Y k_q^Y(v) \, Y \, N(B;v) \\
& -\sum_Y \sum_{\Delta v} k_V^Y(v \rightarrow v + \Delta v) \, Y \, N(B;v) \\
& +\sum_Y \sum_{\Delta v} k_V^Y(v + \Delta v \rightarrow v) \, Y \, N(B;v + \Delta v)
\end{aligned} \tag{11}$$

where S is the amplitude of the pumping term that can be assumed to be a delta function centered at $t = 0$ if the pulse width is short compared to the energy transfer time scale. Also, the number of excited B-states species is so small compared to the number of ground state species that only B-X collisions occur. Summing over Y accounts for energy transfer with multiple buffer

species. The last term allows for transfer into the observed level from all other levels. This equation can be written more concisely with notation, also from Perram [12] as

$$dN_p/dt = S\delta_{pp_o} + R_{pq}N_q \qquad (12)$$

where

$p = (B;v)$ label for the observed vibrational level

$p_o = (B;v_o)$ label for the parent vibrational level

$q = (v + \Delta v)$ label for the indexed vibrational level

$w_{pq} = \sum_Y k_V^Y(q \rightarrow p)\, Y$, the $V \rightarrow T$ rate constant from $q \rightarrow p$

$$R_{pq} = w_{pq} - \delta_{pq}\left(\sum_l w_{lp} + \Gamma_o(p) + \sum_Y k_q^Y(p)\, Y\right)$$

the energy transfer rate matrix connecting state q to state p

δ = Kronecker delta function

2.4.3 Time Dependent Solutions

For a pulsed excitation source with a short pulse width compared to the to the shortest excited state lifetime, the source term S and delta function can be omitted and replaced by the initial condition

$$N(v')_{t=0} = \delta_{vv_o} N(v_o')_{t=0} \qquad (13)$$

If the number density is normalized to the number initially pumped, the master rate equation, Eq (12), becomes

$$dx_p/dt = R_{pq}x_q \qquad (14)$$

where

$$x_p(0) = \delta_{pp_o} \qquad \text{and} \qquad x_p = N_p/N_{p_o} \ (t = 0)$$

This describes the population time evolution of an excited state, x_p , after an initial population is created in state x_{p_o} by a pulsed laser source.

2.4.4 Electronic Quenching

The most elementary pulsed LIF experiment is to measure the time profile of the total fluorescence as a function of the buffer gas pressure. This will produce the electronic quenching rate of the excited state. If thermalization occurs rapidly, then the fluorescence observed is from all excited vibrational levels. If the excited state lifetime and quenching rate are independent of vibrational level, then by defining

$$x_T = \sum_p x_p \tag{15}$$

Eq (11) becomes

$$dx_T/dt = -\left(\Gamma_o + \sum_Y k_q^Y \, Y \right) x_T \tag{16}$$

where the last two terms exactly cancel if the detector efficiency is uniform for all vibrational levels. The solution to Eq (16) is

$$x_T = \exp(-t/\tau) \qquad \text{or} \qquad \ln(x_T) = -t/\tau \tag{17}$$

where

$$1/\tau \ = \ \Gamma_o(p) + \sum_Y k_q^Y \, Y \tag{18}$$

A plot of Eq (18) versus buffer gas pressure is the Stern-Volmer technique and yields the total quenching rate and the collision-free lifetime. This is how k_q was found in previous experiments.

2.4.5 Landau-Teller Scaling

Landau and Teller [9] used first order perturbation theory to describe vibrational relaxation. The transition probabilities, and therefore the rate constant, scale by vibrational level as

$$k_v(v', v'-1) = v' \cdot k_v(1,0)$$
$$|\Delta v| = 1 \text{ only}$$

(19)

with transitions restricted to adjacent states because of modeling the system as a harmonic oscillator.[12]

2.4.6 Detailed Balance

The principle of detailed balance states that at equilibrium, the rate of transfer into an energy level must equal the rate out of that energy level. Since the population of the upper level obeys the Boltzmann distribution, then an upward transition is slower such that

$$k_v(v'-1, v') = k_v(v', v'-1) \exp\left(-\Delta E_{v', v'-1}/k_B T\right)$$
$$\text{and}$$
$$k_v(v'-1, v') = v' \cdot k_v(1,0) \exp\left(-\Delta E_{v', v'-1}/k_B T\right)$$

(20)

2.4.7 Montroll-Shuler Model

Another approach that yields an analytic solution to the problem of vibrational relaxation is found by transforming the population $x_p(t)$ by

$$z_p(t) = x_p(t) \exp(t/\tau)$$

where

(21)

$$1/\tau = \Gamma = 1/\tau_r + \sum_Y k_q^Y Y$$

This changes the time dependent master rate equation, Eq (12), to

$$dz_p/dt = k_v^M(1,0)\left\{pe^{-\Theta}z_{p-1} - \left[p+(p+1)e^{-\Theta}\right]z_p + (p+1)z_{p+1}\right\} \qquad (22)$$

where
$$\Theta = h\upsilon/k_B T$$

If a particular state, q , is populated instantaneously at time t=0, then the Montroll-Shuler[11] solution to Eq (22) for the population in state p is

$$x_p(t) = \frac{(1-e^{\Theta})\,e^{q\Theta}e^{-\Gamma t}}{(e^{-t'}-e^{\Theta})}\left(\frac{e^{-t'}-1}{e^{-t'}-e^{\Theta}}\right)^{p+q} F(-p,-q,1;u^2) \qquad (23)$$

where

υ = the fundamental vibrational frequency

$t' = t\left(1-e^{\Theta}\right)\Gamma_v$

$\Gamma_v = \sum_Y k_v^Y(1,0)\,Y$

$u = \sinh(\Theta/2)/\sinh(t'/2)$

F = hypergeometric function

The Montroll-Shuler model for harmonic oscillators makes the following assumptions:

1. Transitions involving only $|\Delta v| = 1$ are allowed;

2. Landau-Teller scaling of $V \rightarrow T$ transfer rates with vibrational quantum number is applied;

3. Detailed balance is used to relate upward and downward transfer rates;

4. Radiative lifetimes and electronic quenching rates are independent of vibrational level.

The biggest advantage of the Montroll-Shuler is that only a single temporal profile from a collisionally populated vibrational state is needed to obtain a value for $k_v^\gamma(1,0)$, and hence the entire rate matrix R_{pq}. Its implementation with the experiment is found in Appendix A.

Some of the previous assumptions are open to question. The anharmonicity, $\omega_e\chi_e/\omega_e$, of Br_2 is shown in Table 1. It is nearly as low as IF and BrF which are adequately described by the Montroll-Shuler model,[10,17] and lower than BrCl which deviates slightly from the M-S prediction.[12] However, the study only considers the $v' \leq 4$ states, which are in a fairly harmonic region of the potential curve. For now, it is reasonable to assume that the radiative lifetimes and electronic quenching rates are independent of vibrational level. The most questionable assumption is of $|\Delta v| = 1$. BrCl(B), which has a vibrational level spacing relative to kT of ≈ 1 and is higher than Br_2(B), has multi-quantum transfer rates as high as 40% of that for $\Delta v' = -1$.[12]

Table 1. Halogen/Interhalogen Anharmonicity and Vibrational Spacing.[17,10,12,8]

	IF(B)	BrF(B)	BrCl(B)	Br_2(B)
$\omega_e\chi_e/\omega_e$	0.007	0.009	0.013	0.010
$\Delta E/k_BT$	2.0	1.7	1.1	0.655

2.4.8 SSH Theory

The Schwartz, Slawsky, and Herzfeld (SSH) Theory[15] is explained in Appendix A, but its primary result is that the logarithm of the vibrational transfer probability due to collisions is proportional to the reduced mass of the collision partners to the 1/3 power.

$$\ln(P_{10}) = A - B\mu^{1/3} \tag{24}$$

This assumption is based on the vibrational energy spacing being relatively large, which was previously shown not to be the case. This turned out to work for IF(B) and BrF(B), but not for BrCl(B) and $Br_2(B)$.[17,10,14,12,8] This scaling, however, should help in determining if additional V-V transfer occurs in $Br_2(B)$ with molecular buffer gases when compared to the previous $Br_2(B)$ data.[8]

2.5 Experimental Approach

To apply the Montroll-Shuler model to the experiment, spectrally and temporally resolved LIF emission traces for both parent and collisionally populated satellite vibrational levels were obtained. The dye laser was tuned to excite a specific vibrational level, and the monochromator was also tuned to observe a collisionally populated satellite level only. These excitation and observation wavelengths were found by Holmberg [8] through laser excitation spectra and emission spectra. The spectrally resolved emissions were collected by a photomultiplier tube, amplified, sent to a digital oscilloscope, and averaged over 2000 laser pulses. This procedure was done for each molecular buffer gas through a range of pressures.

III. Description of Experiment

3.1 Experimental Setup

The apparatus used in this is experiment is shown in Figure 6. The test cell was a 7.2 cm diameter, 20 cm long glass cell with two 1/2" diameter glass tube ports located at the ends of the cell for the laser path. These ports had 2.5 cm diameter quartz Brewester angle windows to reduce r   ction loss. Additionally, the cell contained two 5 cm diameter observation ports for collection of side fluorescence, one of which was used for vibrationally resolved fluorescence. The cell had two other ports for the vacuum and gas handling system, and one other port for a temperature gauge. All vacuum system connections were made with 1/2" inch Cajon Ultratorr connectors. An Acatel model 200 direct drive chemical plasma pump was used to evacuate the cell. Preceding the pump were two liquid nitrogen cold traps to capture the Br_2. Both an MKS model 122a, 10 torr head capacitance manometer and an MKS model 390, 1 torr head capacitance manometer were used to measure the cell pressure. The cell leak rates plus outgassing rates for the static cell were less than 3 mtorr/hour.
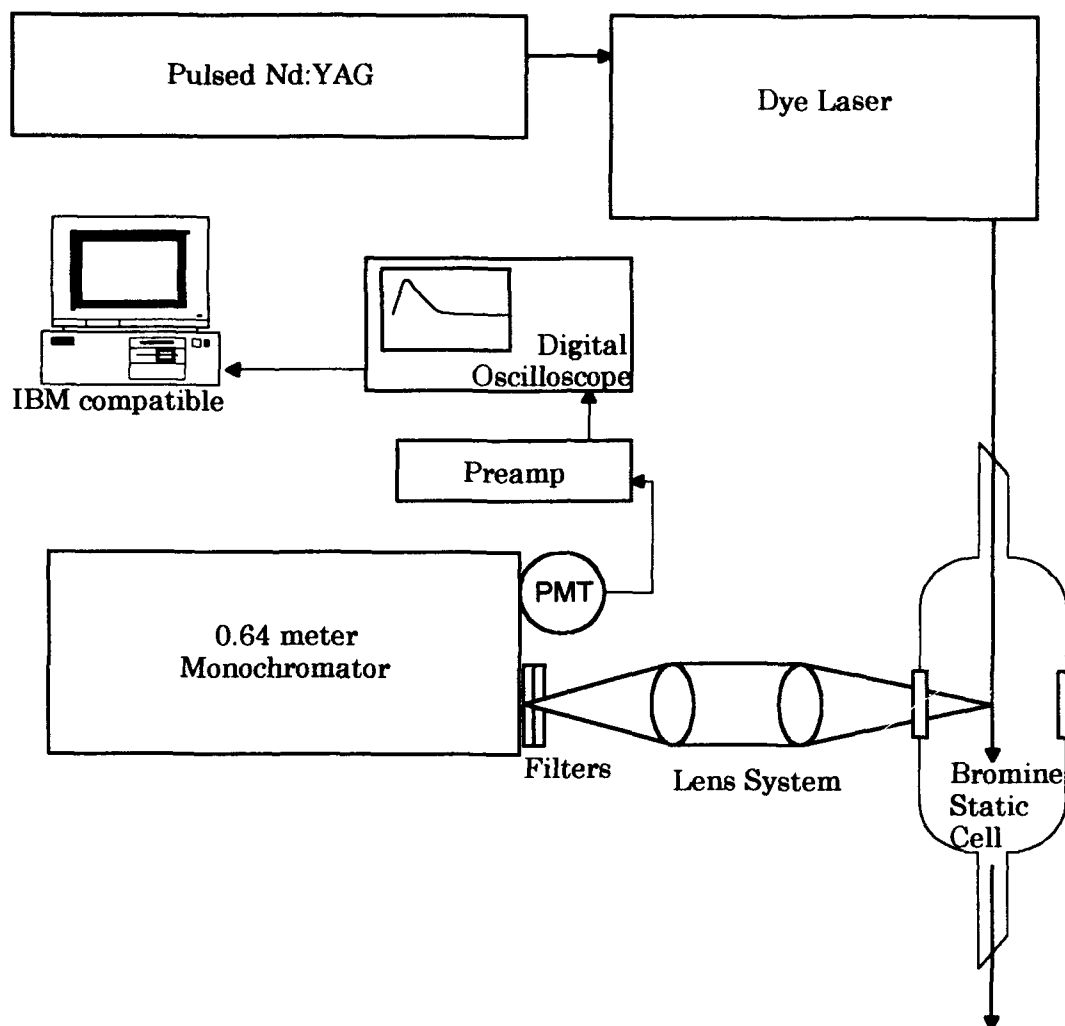
Figure 6. Diagram of the experimental apparatus used to observe pulsed LIF in Br_2.

All experiments were conducted in a static cell filled with small amounts of gaseous Br_2 along with either N_2, O_2, NO, or SF_6. The bromine used was 200ml of 90% atm enriched $^{79}Br_2$ from Icon Co. Isotopically enriched $^{79}Br_2$ was used so that no overlap from $^{81}Br_2$ or $^{79}Br^{81}Br$ would be present in the spectrum. The buffer gases purity and bottler are listed in Table 2.

Table 2. Buffer Gas Data.

Buffer gas	Purity	Bottler
Nitrogen (N_2)	99.999%	Airco
Nitric Oxide (NO)	99.0%	Matheson
Oxygen (O_2)	99.994%	Airco
Sulfur Hexafluoride (SF_6)	99.9%	Airco

3.2 Excitation System

Ground state Br_2 was excited to a specific rovibrational level within the B-state by a Spectra-Physics model PDL-3 pulsed dye laser using LDS 698 dye, which was pumped by a 20 Hz , frequency-doubled Quanta-Ray DCR-3 pulsed Nd:YAG. Specific rovibrational levels in Br_2(B) were populated by tuning the dye laser to a suitable absorption line in the X$\rightarrow$ B transition. The tuning range of the dye was 680-720 nm with an average output power of 5-7 mJ/pulse at 20 Hz, in 10 nanosecond pulses. The linewidth of the pulsed dye laser was 0.07 cm^{-1}. The beam was focused to where it was approximately 1 mm in diameter at the center of the cell.

3.3 Fluorescence Detection System

The laser induced fluorescence (LIF) was detected through one of the two 5 cm Pyrex windows. A two-lens system was used to focus the Br_2 emission onto the entrance slit of an Instruments SA, Inc., HR640 0.64 meter monochromator with a 1200 groove/mm grating. The monochromator had an

RCA C31034 photomultiplier tube (PMT) which detected the emissions in the 560-880 nm wavelength range. The first lens, a 2" diameter, 10 cm focal length, was placed so that the focus was in the path of the laser beam. The second lens, a 2" diameter, 5 cm focal length, was placed such that the focus was centered on the entrance slit. Between the second lens and the slit were Corian long-pass filters that consisted of either two 700 nm filters or a 780 nm filter combined with a 700 nm filter. The entrance slit and exit slits were set to 1 mm to give a resolution of 22.4 Å [10]. The slits and filters were used to minimize the collection of scattered laser light from the dye laser. The PMT output was fed through a PARC model 115 preamplifier and displayed on a LeCroy 9450, 350 MHz oscilloscope. The oscilloscope was pre-triggered by 0.17 μsec and decay profiles of 2-5 μsec were measured with 2000 shot averaging. Collected data was then transferred to a Micro Generation 486DX50 personal computer via a National Instruments AT-GPIB board and a QuickBasic program implemented by Holmberg [8] within the National LabWindows software package.

3.4 Experimental Procedure

Laser excitation of v' = 2 and v' = 3 vibrational levels was accomplished through the (v',v") = (2,4) and (3,5) vibrational transitions. Because of low populations in the v" = 4 and 5 ground states at room temperature, electrical tape was placed around the bromine cell to raise the temperature to 85-102°C, which doubled the population.

Previously determined dye laser wavelengths were tuned to selectively excite $Br_2(X)$ to $Br_2(B)$, and the monochromator was set to observe the collisionally populated emissions. Table 3 summarizes the wavelengths used.

Table 3. Pump and Observation Wavelengths.[8]

	v' = 1	v' = 2	v' = 3
Pump(PDL laser)		6724.1 Å	6796.4 Å
View(Monochromator)	8162.0 Å	7860.0 Å	7425.0 Å

For each buffer gas, spectrally and temporally resolved fluorescence waveforms were recorded as a function of buffer gas partial pressure. For the v' = 3 initially excited case, emissions were observed for v' = 2 and 3, and for the v' = 2 excitation, emissions were observed for v' = 1, 2, and 3. Because of the strong overlap with v' = 2, no isolated emissions from v' = 0 or 4 collisionally populated levels were observed.[8]

Emissions from a collisionally populated state were averaged for 2000 laser pulses. Background subtraction was accomplished by tuning the dye laser away from the parent vibrational level absorption line and then averaging 2000 shots. This method was done for each waveform collected and produced a reasonable signal-to-noise ratio of five. This is much lower than the typical signal-to-noise ratio of at least ten by Holmberg [8], and can be attributed to the reduced power output of the Nd:YAG laser. It produced 5-7 mJ/pulse at the exit of the dye laser compared to an earlier 20 mJ/pulse. This is also the same reason that the waveform had to be averaged over 2000 pulses rather than the previous 1000.

The first task to accomplish before collecting new data was to try to replicate Holmberg's experimental runs with $Br_2(X)$ and then argon as the collision partner. After successfully completing this with less power, the molecular buffer gases were then analyzed.

The procedure for this was to add a small amount of Br_2 to the cell and then add the specific buffer gas and record the waveform profile as a function of buffer gas pressure (or concentration). For each set of waveforms recorded, the bromine concentration remained the same while the buffer gas concentration was increased. The waveform was analyzed by fitting the data to the Montroll-Shuler model that was implemented in the TableCurve software package from Jandel Scientific as a user defined function (see Appendix A). Each fitted waveform was returned from TableCurve with two energy transfer parameters that were found. These values were

$$\Gamma_v = \sum_Y k_v^Y(1,0)\, Y$$
$$\Gamma_q = 1/\tau_q = 1/\tau_o + \sum_Y k_q^Y\, Y \tag{25}$$

By plotting the fundamental vibrational rate, Γ_v, versus the buffer gas pressure, the fundamental vibrational rate coefficient, $k_v(1,0)$, is found as the slope. Similarly, the vibrationally independent quenching rate, k_q, is found when plotting the electronic removal rate, Γ_q, versus buffer gas pressure. This is know as the Stern-Volmer technique.

When the only gas present in the cell is $Br_2(X)$, the inversion of the collision-free lifetime, $1/\tau_o$, is the zero-pressure intercept of the electronic removal rate. If there is no predissociation, then this value is the inversion of the radiative lifetime, $1/\tau_r$. Because of the large extrapolations with respect to buffer gas pressure, the inherent systematic error precluded accurate

determination of these values when only $Br_2(X)$ was the collision partner. With the addition of another buffer gas, the intercept is the collision-free lifetime plus the electronic removal rate for $Br_2(B)$ at that particular pressure.

$$\Gamma_q = 1/\tau_q = (1/\tau_o + k_q[Br]) + k_q Y \qquad (26)$$

When taking data with only $Br_2(X)$ as the collision partner, the ideal intercept of Γ_v vs. Y should be zero; however, factors such as overlap from competing vibrational bands and differences in vibrational level quenching rates and radiative lifetimes caused positive intercepts. When using a buffer gas as the collision partner, the intercept will be the fundamental vibrational rate, Γ_v, for bromine at that particular concentration.

$$\Gamma_V = (k_v^{Br}(1,0) [Br]) + k_v^Y(1,0) Y \qquad (27)$$

The addition of buffer gas will produce a fundamental vibrational rate coefficient, $k_v(1,0)$, for $Br_2(B)$ with that particular gas. A unique electronic quenching rate is also found for the particular observation level.

24

IV. Results and Discussion

4.1 V→T Transfer With N_2 as the Collision Partner

Vibrationally resolved fluorescence decay profiles were obtained from v' = 2 and 3 for the v' = 3 initially populated, and from v' = 1, 2, and 3 for the initially populated v' = 2. Fluorescence decay profiles were recorded as a function of N_2 partial pressure. The range of the Br_2 pressure went from 0.5-1.0 Torr while the N_2 partial pressures included 0-5.0 Torr.

When observing the satellite populated states, the majority of the data collected had its N_2 pressure below 3 Torr. The pressure could be increased higher for p2v1 (pump v'- 2, view v'=1) and p2v3 than p3v2 because of the longer time profile for these states. Because of the strong signal from the parent level, pressures for N_2 in the p3v3 and p2v2 data runs went from 0-1 Torr with 400 mTorr of Br_2.

Low Br_2 pressure limits were picked to provide a waveform that had a fairly good signal-to-noise ratio. Generally speaking, the p3v2 data had the strongest and clearest signal, the p2v1 data came next, and the p2v3 data had the lowest signal-to-noise ratio, which was attributed to having to use a different filter so that the signal could be seen. The p2v3 data had much noise from the laser pulse that could not be filtered out.

Typical fluorescence decay profiles are shown in Figure 7 and Figure 8 after initially populating v'=2. The first profile is of an observed parent vibrational level v'=2 at a Br_2 pressure of 750 mTorr, and the second is of vibrationally populated satellite states v'=1 and 3. The relatively short time

25

scales indicate that $Br_2(B)$ has a short radiative lifetime and that the electronic quenching may contribute significantly to its decay. The longer profile for v'=1 compared to v'=3 also shows that the vibrational transfer out of a state increases with increasing vibrational quantum number.

4.1.1 Montroll-Shuler Fits

All observed fluorescence waveforms were analyzed with the implementation of the Montroll-Shuler model in TableCurve. Although some of the assumptions of the Montroll-Shuler model are questionable for the specific case of $Br_2(B)$, it is the only analytic solution to the master rate equation for vibrational transfer. Typical fits to collisionally populated satellite states with N_2 as the buffer gas are shown in Figures 9-14. The fits for all data were very good and will be discussed later.
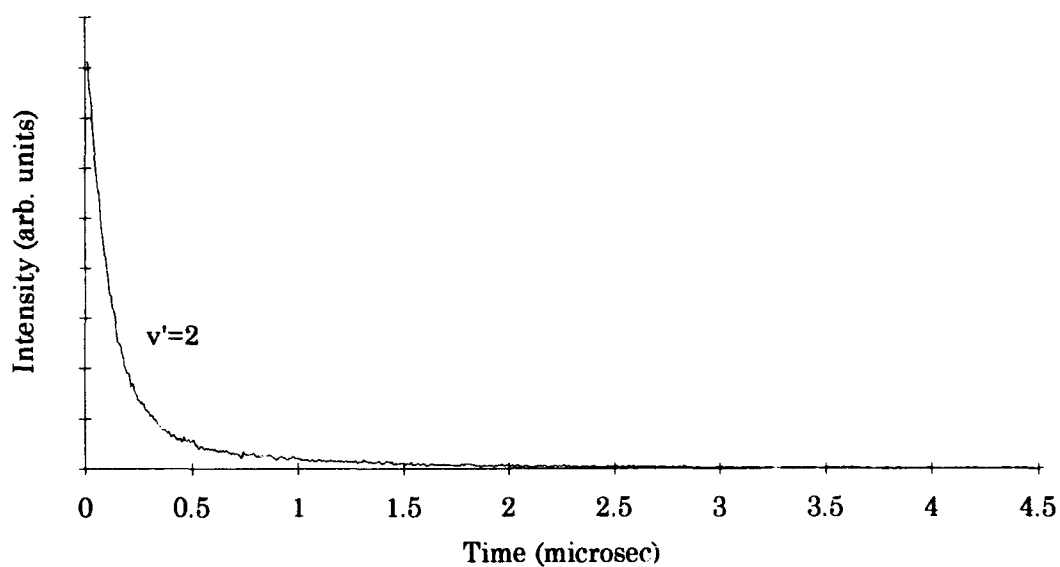
Figure 7. Spectrally resolved, temporally resolved fluorescence profiles for v'=2 after initial excitation of v'=2 at 750 mTorr of Br_2.
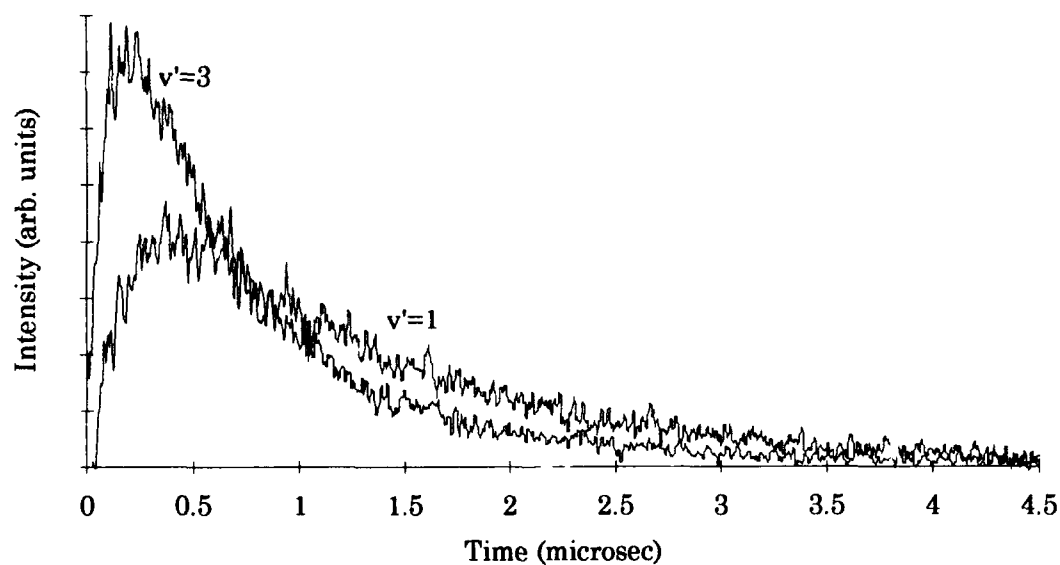
Figure 8. Spectrally resolved, temporally resolved fluorescence profiles for v'=1 and v'=3 after initial excitation of v'=2 at 750 mTorr of Br_2.
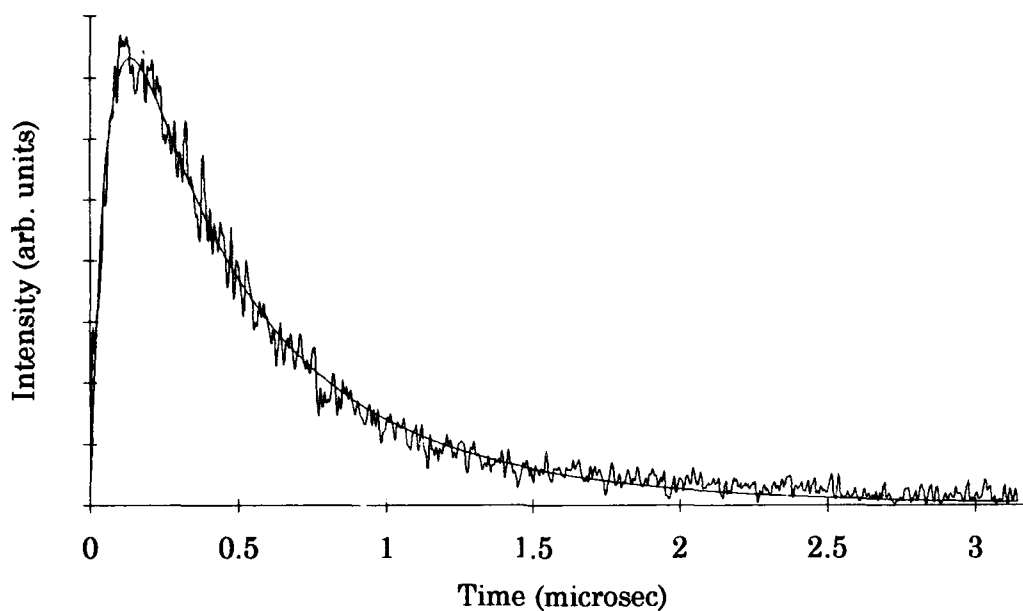
Figure 9. Montroll-Shuler fit to emissions from the (2-11) band transition after initial excitation of v'=3 (p3v2) with a Br_2 pressure of 802 mTorr and N_2 pressure of 788 mTorr.
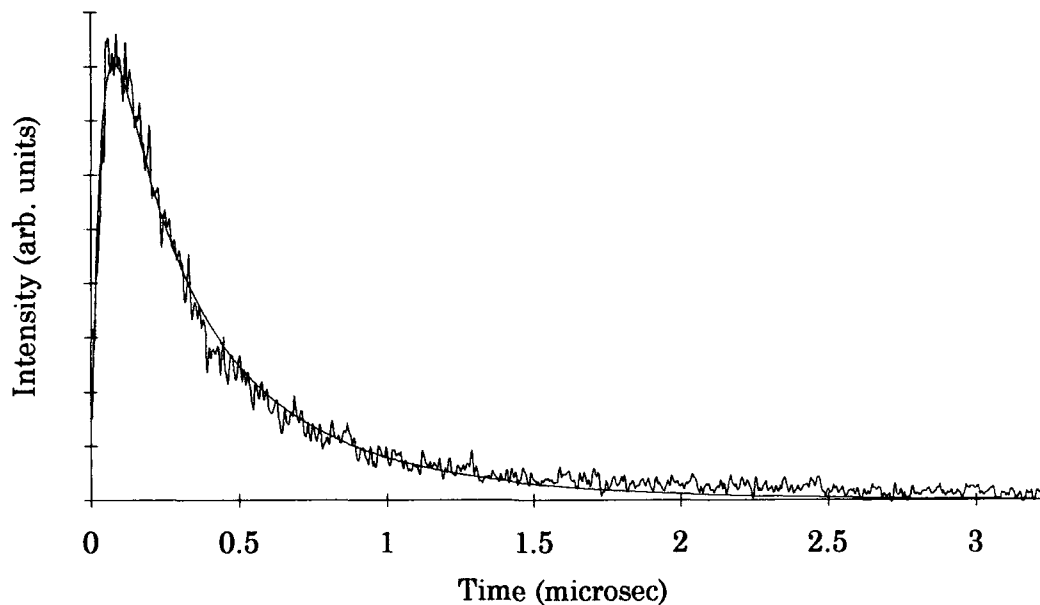
Figure 10. Montroll-Shuler fit to emissions from the (2-11) band transition after initial excitation of v'=3 (p3v2) with a Br_2 pressure of 802 mTorr and N_2 pressure of 2397 mTorr.
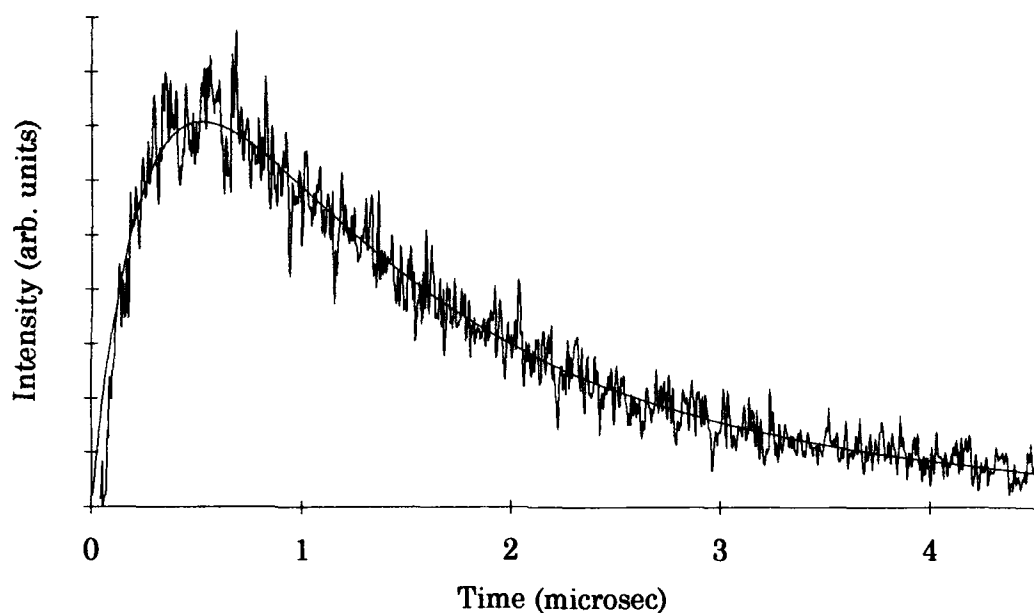
Figure 11. Montroll-Shuler fit to emissions from the (1-11) band transition after initial excitation of v'=2 (p2v1) with a Br_2 pressure of 500 mTorr and N_2 pressure of 264 mTorr.
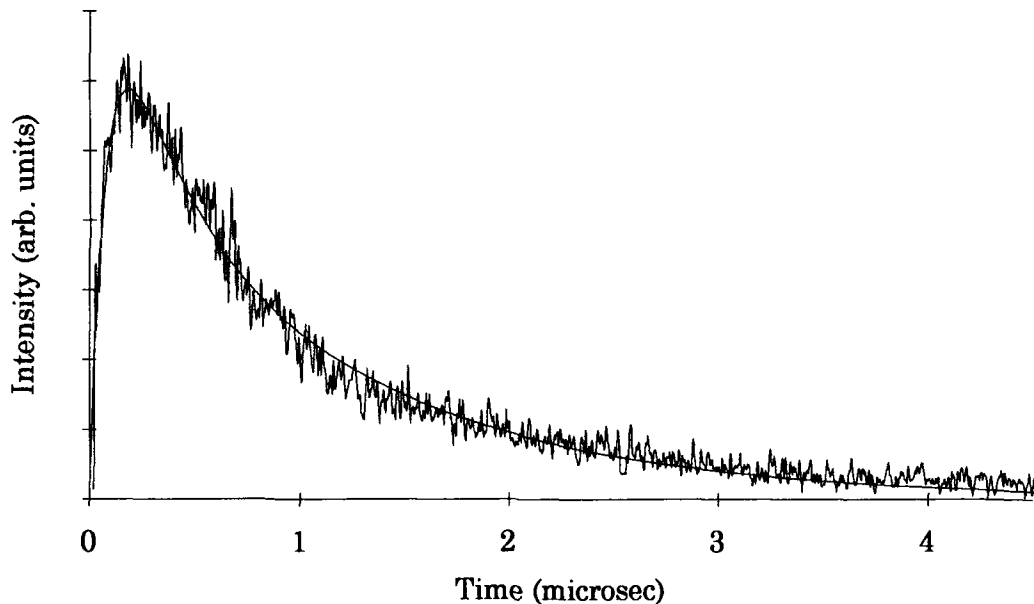
Figure 12. Montroll-Shuler fit to emissions from the (1-11) band transition after initial excitation of v'=2 (p2v1) with a Br_2 pressure of 500 mTorr and N_2 pressure of 2889 mTorr.
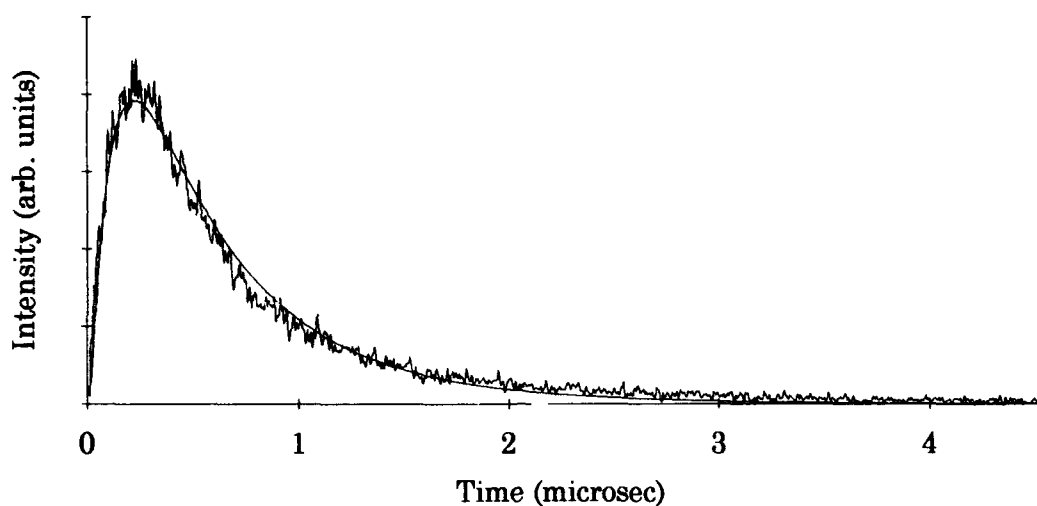
Figure 13. Montroll-Shuler fit to emissions from the (3-9) band transition after initial excitation of v'=2 (p2v3) with a Br_2 pressure of 570 mTorr and N_2 pressure of 227 mTorr.
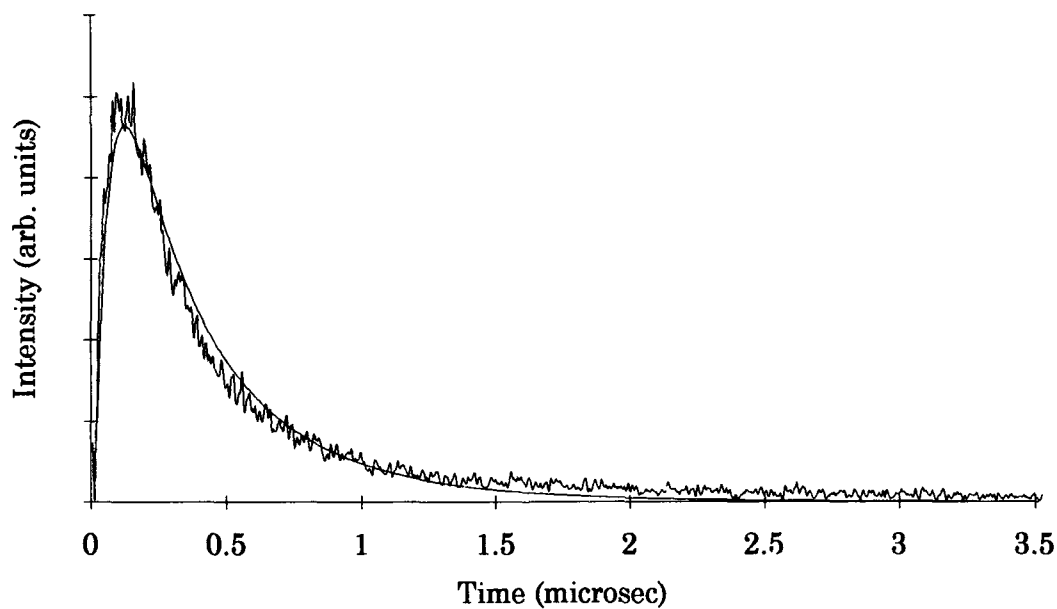
Figure 14. Montroll-Shuler fit to emissions from the (3-9) band transition after initial excitation of v'=2 (p2v3) with a Br_2 pressure of 500 mTorr and N_2 pressure of 1835 mTorr.

4.1.2 Stern-Volmer Analysis

As discussed earlier, data was collected for observation bands over a range of pressures. The resulting energy transfer parameters, Γ_v and Γ_q were plotted against the buffer gas pressure to yield $k_v(1,0)$ and k_q. Figures 15 and 16 show results for $k_v(1,0)$ and k_q, respectively, from two different pump v'=3, view v'=2 experiments with N_2 as a collision partner.

Since each data run had a unique Br_2 pressure, the raw data for all runs of each observation level could not be combined to find a singular slope; however, the slopes of the Stern-Volmer plots should be the same, so they were averaged. The same analysis technique was accomplished on each pump-view level combination. The weighted average results of each observed vibrational level for $k_v(1,0)$ and k_q with N_2 as the collision partner, are presented in Table 4. The error quoted in Table 4 is explained in Appendix B.

Table 4. Fundamental vibrational transfer rate coefficients and electronic quenching rate coefficients ($10^{-11} cm^3/molec \cdot sec$) from $Br_2(B)$ collisions with N_2. Note that $k_v(p,v) = k_v(2,3)$ for pump v' = 2, view v' = 3.

v' pump/ view	$k_v(1,0)$	$k_v(p,v)$	k_q
2 / 3	3.5 ± 0.4	5.5 ± 0.6	2.1 ± 0.6
3 / 2	3.5 ± 0.1	10.6 ± 0.4	0.72 ± 0.04
2 / 1	2.5 ± 0.4	4.9 ± 0.9	0.4 ± 0.1
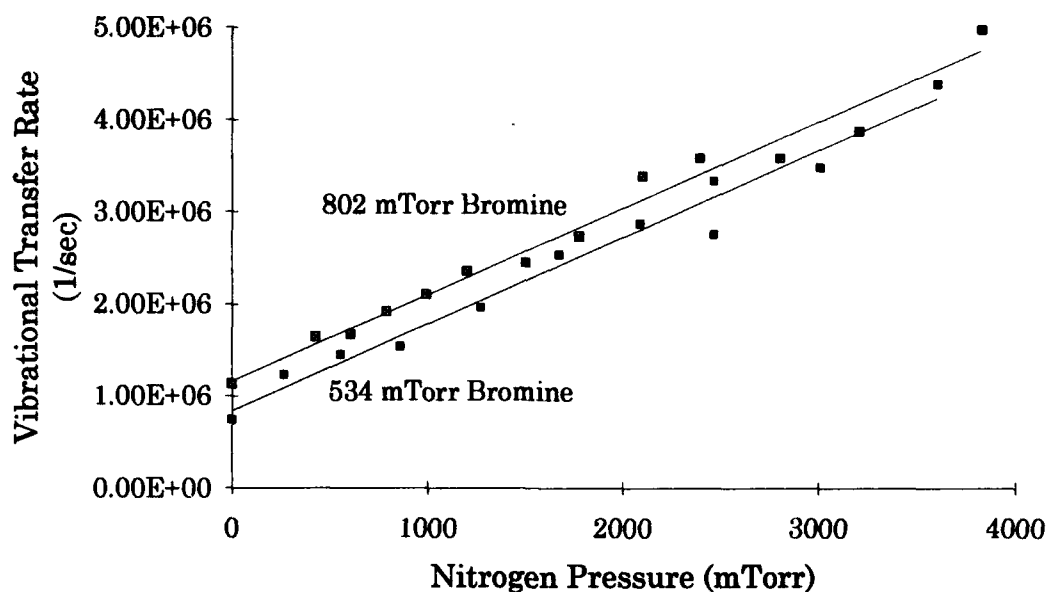
Figure 15. Stern-Volmer plot of the Montroll-Shuler vibrational transfer fits to two pump v'=3, view v'=2 data with N_2 buffer gas that gives $k_v(1,0)=3.5 \ (\pm 0.1) \times 10^{-11} \ cm^3/molec\text{-}sec$.
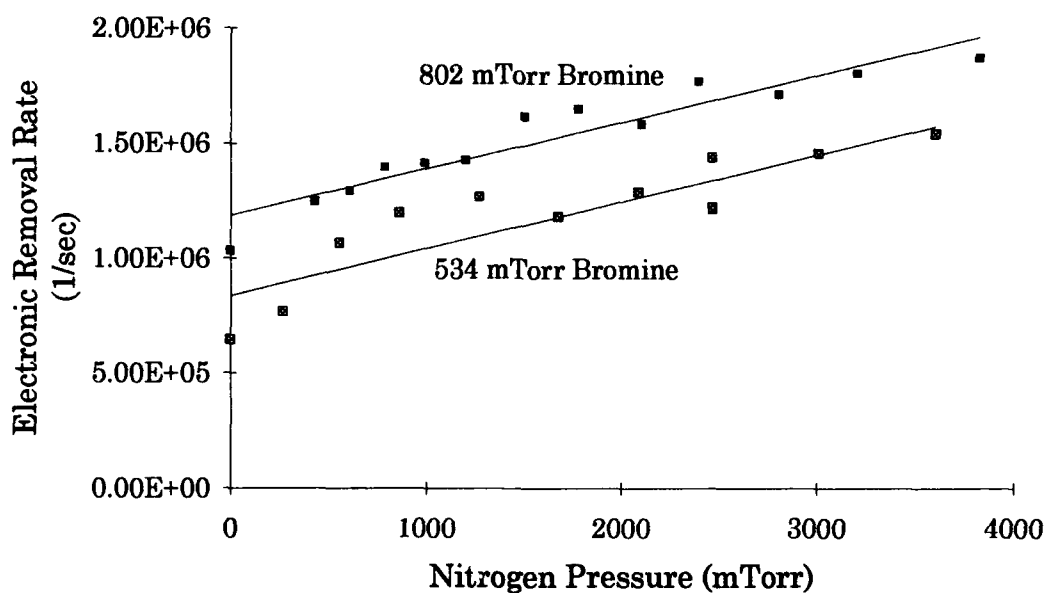
Figure 16. Stern-Volmer plot of the Montroll-Shuler electronic quenching fits to two pump v'=3, view v'=2 data with N_2 buffer gas that gives $k_q = 7.2 \ (\pm 0.4) \times 10^{-12} \ cm^3/molec\text{-}sec$.

32

4.2 V→T Transfer With O_2, NO, and SF_6 as Collision Partner

Vibrational transfer studies were also accomplished with O_2, NO, and SF_6 as collision partners. These molecules were chosen because they did not react with Br_2, and their results could be compared to previous interhalogen vibrational transfer studies. Also, the molecular weight of NO is between N_2 and O_2, which is useful when analyzing the SSH theory. O_2 was studied as extensively as N_2, and the same types of results are presented. Nitric oxide, because of its toxicity, was studied less with only three p3v2 and one p2v1 experiments conducted. Sulfur hexafluoride had the exact number and type of runs as NO, and was used to see if the extra degrees of freedom would produce more V-V transfer. Data was not taken for parent level emission for any of the remaining gases.

4.2.1 Oxygen

Oxygen was studied almost as thoroughly as nitrogen so that the two diatomic molecules could be compared to each other. The pressure of Br_2 was from 0.5–0.8 Torr with the partial pressure of O_2 varying from 0–3.5 Torr. This pressure was lower than N_2 because as the experimental technique for collecting data was improved, data taken for pressures higher than 4 Torr was not needed.

The analysis for the data was the same as before with the waveform being fit to the Montroll-Shuler model, the appropriate parameters being graphed as a function of buffer gas partial pressure, and the vibrational rate coefficients being extracted from the Stern-Volmer plots. Typical curve fits for the remaining buffer gas partners are shown in Appendix C. The rate

coefficients for each observed vibrational level are shown in Table 5, with the error explained in Appendix B.

Table 5. Fundamental vibrational transfer rate coefficients and electronic quenching rate coefficients (10^{-11}cm^3/molec·sec) from Br_2(B) collisions with O_2. Note that k_v(p,v) = k_v(2,3) for pump v' = 2, view v' = 3.

v' pump/ view	k_v(1,0)	k_v(p,v)	k_q
2 / 3	2.8 ± 0.7	4.3 ± 1.1	3.4 ± 0.4
3 / 2	3.3 ± 0.5	10.0 ± 1.6	1.5 ± 0.2
2 / 1	2.4 ± 0.5	4.7 ± 0.9	0.57± 0.01

4.2.2   Nitric Oxide (NO) and Sulfur Hexafluoride (SF$_6$)

Nitric oxide data was taken for only p3v2, and it fit the Montroll-Shuler model very well. The pressures for Br_2 were from 0.4 – 1.0 Torr while the pressures for NO and SF$_6$ were from 0 – 2.1 Torr. SF$_6$ data was taken to investigate whether the extra degrees of freedom would produce more V-V transfer. After examining the p3v2 data and concluding that this did not happen, only one p2v1 run was recorded. The results for NO and SF$_6$ are shown in Table 6, and sample Montroll-Shuler fits along with Stern-Volmer plots are in Appendix C.

34

Table 6. Fundamental vibrational transfer rate coefficients and electronic quenching rate coefficients ($10^{-11} cm^3$/molec·sec) from $Br_2(B)$ collisions with NO and SF_6. Note that $k_v(p,v) = k_v(3,2)$ for pump v' = 3, view v' = 2.

Buffer gas	v' pump/ view	$k_v(1,0)$	$k_v(p,v)$	k_q
NO	3 / 2	4.1 ± 1.1	12.2 ± 3.4	6.9 ± 1.1
NO	2 / 1	2.6 ± 0.4	5.2 ± 0.8	5.0 ± 0.5
SF_6	3 / 2	3.2 ± 1.0	9.6 ± 2.9	1.7 ± 1.1
SF_6	2 / 1	1.5 ± 0.2	3.0 ± 0.3	0.43 ± 0.03

4.3 Discussion of $Br_2(B)$ Vibrational Transfer Results

The results from the previous sections show that the V-T transfer in the lower vibrational levels (v'$\leq$ 4) of the $Br_2(B)$ electronic state for the buffer gases studied is adequately described by the Montroll-Shuler model. The fundamental vibrational transfer rate coefficients and average electronic quenching rate coefficients for each collision partner studied, as well as the rates from Holmberg's experiment are summarized in Table 7. The reported values for all collision partners are from the pump v'=3 and view v'=2 data. If the vibrational rate coefficients are averaged for all the vibrational levels studied, $k_v(1,0)$ for N_2 and O_2 would be 3.4 (±0.6) x 10^{-11} cm^3/molec-sec and 2.9 (±0.6) x $10^{-11} cm^3$/molec-sec respectively. Because of the large difference in values for k_q between vibrational levels in N_2 and O_2 , these values could not be averaged within reasonable error bounds.

Table 7. Fundamental vibrational transfer and electronic quenching rate
coefficients ($10^{-11} cm^3/molec \cdot sec$) for $Br_2(B)$ with various collision partners from
pump v'=3 and view v'=2 data. Values for $Br_2(X)$ and the rare gases are from
reference (8).

Collision Partner	$k_v(1,0)$	k_q	$\sigma_v(1,0)/\sigma_g$
N_2	3.5 ± 0.1	0.72 ± 0.04	.12
NO	4.1 ± 1.1	6.9 ± 1.1	.15
O_2	3.3 ± 0.5	1.5 ± 0.2	.11
SF_6	3.2 ± 1.0	1.7 ± 1.1	.13
$Br_2(X)$	3.6 ± 0.4	5.0 ± 0.1	.20
He	2.5 ± 0.3	0.80 ± 0.12	.048
Ne	2.5 ± 0.2	0.87 ± 0.6	.097
Ar	2.5 ± 0.3	0.50 ± 0.02	.13
Kr	2.8 ± 0.2	0.66 ± 0.8	.15
Xe	3.1 ± 0.4	0.75 ± 0.11	.17

4.3.1 Validity of the Montroll-Shuler Model

The fits of the Montroll-Shuler model to the vibrational transfer data
were very good for all of the observed satellite states for the buffer gases. By
comparing the vibrational rate coefficients in Tables 4, 5, and 6, one finds that
the rates are $\approx 3.0 \times 10^{-11}$ cm^3/molec-sec; however, the $k_v(1,0)$ rate from the
p2v1 data was always below the $k_v(1,0)$ rate from the p3v2 data. This implies
that Landau-Teller scaling may not necessarily apply in this case. Since only
three vibrational levels were observed, no definite conclusions can be drawn.
In the previous experiments of BrF(B) [14,10,16] and IF(B),[17,18] emissions were
observed from several collisionally populated vibrational levels after

excitation of a single parent vibrational level. Although much data was taken from different vibrational levels, noisy data and vibrational overlap prevented excellent fits to the Montroll-Shuler model. Because of overlapping emissions from the parent level with satellite levels at $\Delta v' = \pm 2$, the current experiment was considerably restricted. On the other hand, the relatively strong signals obtained from satellite vibrational levels at $\Delta v' = \pm 1$, which had minimal overlap, more than compensated for the lack of several observed vibrational levels.

The principle of detailed balance is another check on the validity of the Montroll-Shuler model. The $k_v(1,0)$ rates derived from the p3v2 and p2v3 data for both N_2 and O_2 are relatively close and well within experimental error indicating the Montroll-Shuler model does not violate the principle of detailed balance between $v' = 2$ and 3.

4.3.2 Deficiencies with the Montroll-Shuler Model

The assumption of the electronic quenching rate coefficient being independent of vibrational level is clearly seen to be incorrect. While the systematic error for data taken within the specific pump/view level is small, the k_q rates vary from each observed level. The trend is for the quenching to increase with increasing vibrational level.

The Montroll-Shuler fits for the data were very good, but tended to deviate from the data at long times, especially at higher buffer gas pressures. This is even more evident on a logarithmic scale and is shown in Figure 18. Holmberg[8] noted that the deviation was larger for lighter collision partners than the heavier ones. This may not be the case here since the molecular

weights of N_2, O_2, and NO are in between neon and argon. SF_6, however, is in between Br_2 and xenon, but does not necessarily have less deviation from the Montroll-Shuler model than the previous collision partners. The deviation could possibly be explained by multi-quantum transfer and was thought to be the case for helium.[8]

The method for verifying this was to simulate data with a truncated, five-level rate matrix (explained in Appendix A) which assumes that all states greater than $v' = 4$ predissociate. This is an unrealistic assumption, and data generated with the truncated matrix using the rate coefficients obtained from the Montroll-Shuler fit does not go through all of the data past the initial rise. An example of this is shown in Figure 17 and 18 for $f = 0$. Although the truncated matrix did not fit the data, it was used to test the validity of multi-quantum transfer.

The five-level rate matrix was modified to accept a fraction of multi-quantum transfer as an input parameter. This is also explained in Appendix A. For all of the cases tested in N_2 and O_2, the multi-quantum correction factor moved the simulated waveform away from the Montroll-Shuler model fit, which is in the wrong direction. This is also shown in Figures 17 and 18 for $f = 20\%$.
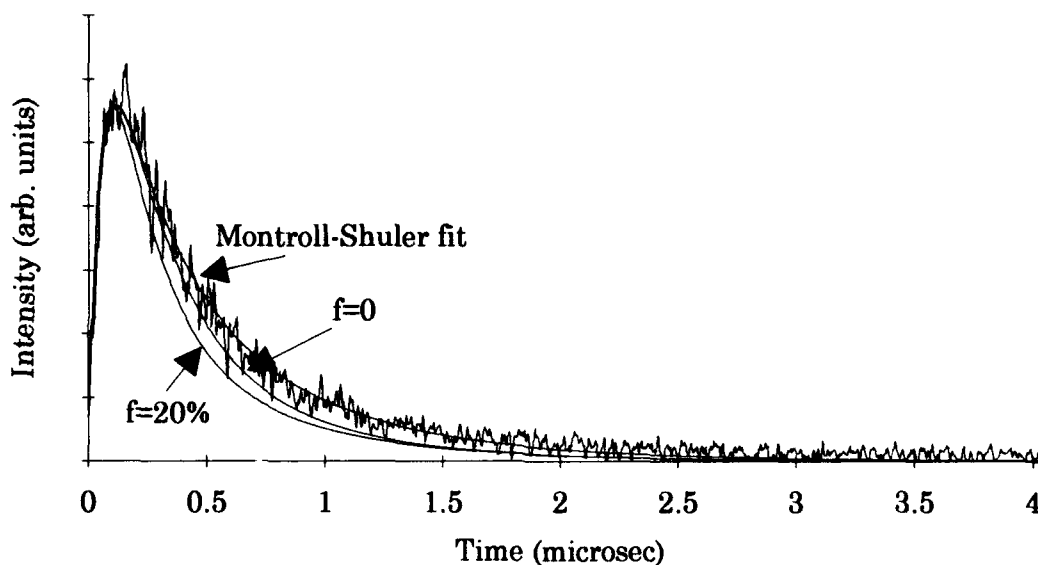
Figure 17. Montroll-Shuler fit and multi-quantum simulated data fits to pump v'=3, view v'=2 with a Br_2 pressure of 704 mTorr and O_2 pressure of 1139 mTorr.
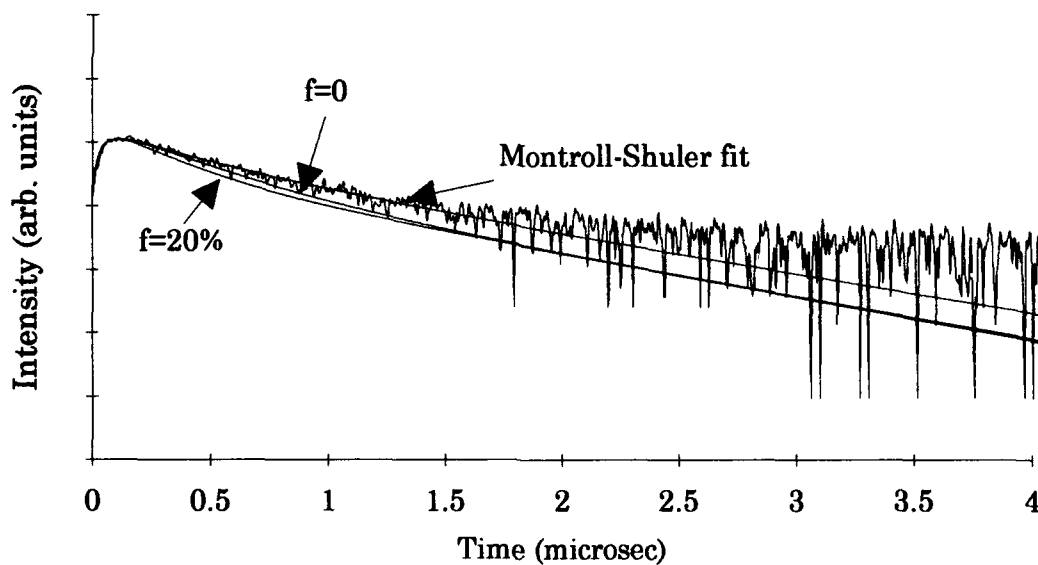
Figure 18. Logarithmic Montroll-Shuler fit and multi-quantum simulated data fits to pump v'=3, view v'=2 with a Br_2 pressure of 704 mTorr and O_2 pressure of 1139 mTorr.

The main fitting error occurs in the tail end of the data where quenching is the primary mechanism. This is also evident in Appendix C, Figures C.21-C.26. For the case of NO, which had a very high k_q value, the fit is very bad as can be seen in Figure C.25. Figures C.21-C.24 also show that the fit is worse at higher buffer gas pressures. This deviation, however, is minor, and Holmberg[8] showed that it did not have a significant effect on the values obtained for the vibrational rate coefficients. He also showed that the quenching term can be described as an "effective" quenching term that increases as each vibrational level gets closer to the predissociation level.[8]

4.4 V→T Scaling Theories

The quantum mechanical Schwartz, Slawsky, and Herzfeld (SSH) theory,[15] described in Appendix A, predicts that the vibrational transfer probability depends upon the reduced mass of the collision partners. If the vibrational energy spacings are large, then the exponential term dominates the expression, and the logarithm of the probability is proportional to $\mu^{1/3}$,

$$\ln\left(\sigma_v(1,0)/\sigma_g\right) = A - B\,\mu^{1/3} \qquad (28)$$

where

$\sigma_v(1,0)/\sigma_g$ = ratio of fundamental vibrational transfer cross-section to the gas kinetic cross-section

A, B = constants independent of reduced mass or energy spacing

The gas kinetic rate is also explained in Appendix A. Table 7 shows the ratio $\sigma_v(1,0)/\sigma_g$ for the buffer gases used in this experiment as well as from the data from collisions with the rare gases. Holmberg [8] showed that $Br_2(B)$ did

40

not scale inversely with the reduced mass of Br_2 and the rare gases such as IF(B) and BrF(B),[17,10,14] but that it scaled linearly with a positive slope. According to Figure 19 , the molecular buffer gases fall along the same line as with the rare gases, so significant V-V transfer is unlikely.

Another reason to suspect minimal V-V transfer is the large vibrational energy spacings of the diatomic buffer gases. The energy spacings of N_2 ,O_2 , and NO are 2360 cm^{-1}, 1580 cm^{-1}, and 1904 cm^{-1} respectively [6]. Since the spacing of Br_2(B) is 170 cm^{-1}, [6] the only way for V-V transfer to occur is for multi-quantum jumps in the B-state. Since the majority of levels above v'=4 predissociate, these multi-quantum jumps will not be observed.
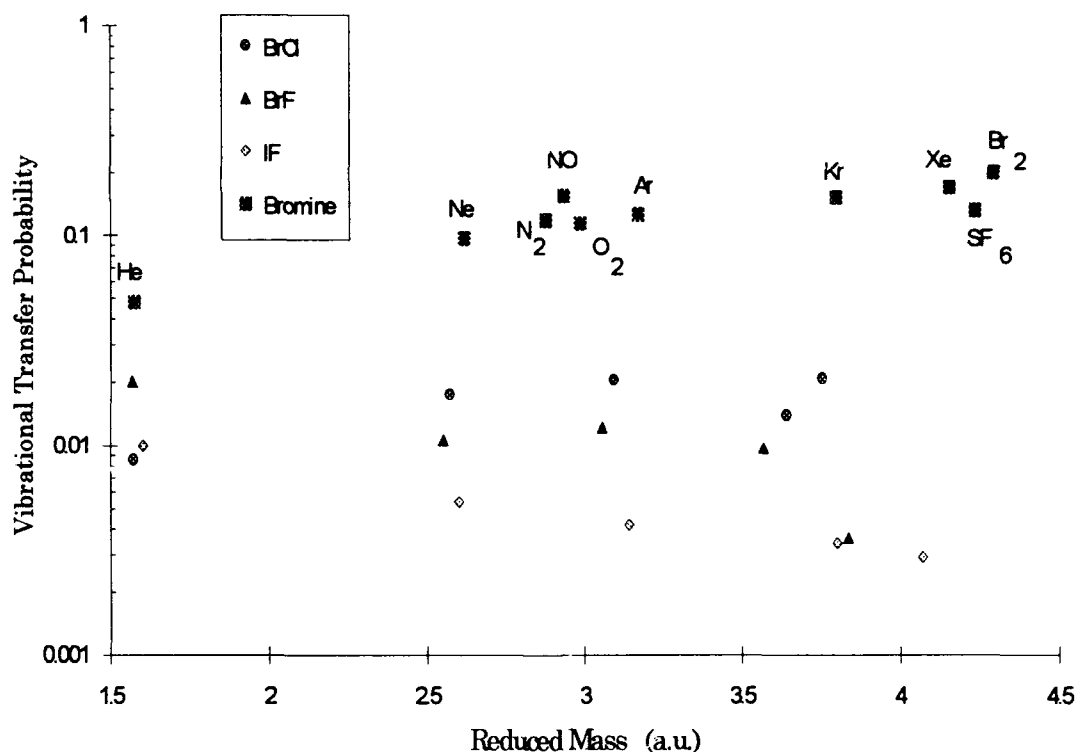

Figure 19. Vibrational transfer probabilities for Br_2 , BrCl, BrF, and IF with rare gas and molecular partners as a function of collision pair reduced mass$^{1/3}$. [8]

41

4.5 Comparison with Previous Studies

Holmberg's experiment with $Br_2(X)$ and the rare gases is the only other spectrally resolved, temporally resolved LIF studies investigating state-to-state vibrational energy transfer in the $Br_2(B)$ state. The vibrational rate coefficients are relatively close to each other for the rare gases and the gases just studied. Clyne, Heaven, and Davis (3) used CW LIF to examine vibrational transfer in $Br_2(B)$ from v'=11 to v'=10 with N_2 as the collision partner and had a reported rate of $k_v(11,10)$=2.5 ($\pm$1.0) x 10^{-11} cm^3/molec-sec. This is not of the same magnitude as the present rate when using Landau-Teller scaling for vibrational transfer. Landau-Teller scaling is applicable to an upper limit that does not exceed the gas-kinetic collision rate. In other words, there cannot exist a V-T transfer rate that is faster than the actual collision rate. If the $k_v(1,0)$ rate found is scaled up to $k_v(11,10)$, then that rate exceeds the gas-kinetic limit.

Clyne, Heaven, and Martinez used temporally resolved total fluorescence emissions from $Br_2(B, v'=2)$ in pulsed LIF experiments to study electronic quenching of N_2, and found an approximate value of k_q =1.0 x 10^{-11} cm^3/molec·sec.[1] Their data is in close agreement with k_q = 0.72 x 10^{-11} cm^3/molec·sec, especially considering that it was taken with a maximum N_2 pressure of 56 mTorr.

Other interhalogen studies with IF(B) and N_2 and O_2,[18] show that the vibrational rate coefficients are at least an order of magnitude slower than with $Br_2(B)$ if Landau-Teller scaling is used. The logarithmic plot of vibrational probabilities versus $\mu^{1/3}$ for IF(B) with N_2 and O_2 showed a significant increase in the vibrational transfer over that for the rare gases.

This was attributed to either V-T or R-T energy transfer, but could also be V-V transfer. For the present study, V-V transfer was found to be insignificant.

In another interhalogen studied, Melton[10] showed that the vibrational transfer rate for BrF(B) with SF_6 as a collision partner was on the order of 10^{-11} cm^3/molec-sec while the quenching rate was on the order of 10^{-14} cm^3/molec-sec. Although BrF and Br_2 have many of the same properties, this did not turn out to be the case for Br_2(B) when combined with SF_6 since the two rates had the same order of magnitude.

V. Conclusions

5.1 Summary of Collisional Energy Transfer in $Br_2(B)$

Vibrational energy transfer and electronic quenching within the nonpredissociative vibrational levels of the $Br_2(B)$ state were investigated for N_2, O_2, NO, and SF_6 collision partners using spectrally resolved, temporally resolved LIF techniques. Vibrationally resolved emissions were observed from levels v'=1, 2, and 3 after initially exciting levels v' = 2 and 3. State-to-state vibrational transfer and electronic quenching rate coefficients were found by fitting the emission data to the Montroll-Shuler model for vibrational transfer in harmonic oscillators. An average fundamental vibrational transfer rate coefficient of $k_v(1,0) = 3.4$ (± 0.6) x $10^{-11} cm^3$/molec-sec predicts the vibrational transfer rates for the $0 \leq v' \leq 3$ collisions with N_2, and a rate of $k_v(1,0) = 2.9$ (± 0.6) x $10^{-11} cm^3$/molec-sec for collisions with O_2. Vibrational rates for NO and SF_6 range from 1.5 (± 0.2) x $10^{-11} cm^3$/molec-sec to 4.0 (± 1.1) x 10^{-11} cm^3/molec-sec. Quenching rates were seen to be vibrationally dependent and went from a low of $k_q = 0.4$ (± 0.1) x $10^{-11} cm^3$/molec-sec for N_2 (pump v'=2 , view v'=1) to a high of $k_q = 6.9$ (± 1.1) x $10^{-11} cm^3$/molec-sec for NO (pump v'=3, view v'=2). The trend was for the quenching to increase with increasing vibrational level.

The Montroll-Shuler model for vibrational energy transfer was good at describing the energy transfer within $Br_2(B)$ with the molecular collision partners of N_2, O_2, NO, and SF_6. At high pressures, however, the Montroll-Shuler model deviated from the observed waveforms for all the buffer gases.

A possible explanation for this is multi-quantum transfer, but cannot be confirmed with current analysis techniques. In any event, the deviation does not have that much of an effect on the vibrational rate coefficient values obtained.

The probability of vibrational transfer in $Br_2(B)$ with N_2, O_2, NO, and SF_6 did not scale with a negative slope according to the SSH theory, but did scale linearly with a positive slope along the same line as the rare gas data. Thus, it can be concluded that V-V transfer is probably insignificant.

5.2 Recommendations

Further study should concentrate on finding an analytical solution to the master rate equation that includes multi-quantum transfer. This most likely is a purely mathematical problem, and needs to be addressed to find an accurate solution for the observed temporal profiles at longer times. To further verify the quenching rates obtained, total fluorescence data should be taken. Finally, vibrational-vibrational energy transfer should be studied with molecular species that have the same vibrational spacing as $Br_2(B)$.

Bibliography

1. Clyne, M. A. A., M. C. Heaven and E. Martinez. "Kinetics of Excited States using Laser Excitation," *Journal of the Chemical Society Faraday Transactions II* 76: 405-419 (1980).

2. Clyne, M. A. A., M. C. Heaven and J. Tellinghuisen. "Theoretical Treatment of the Spontaneous Predissociation of Br_2 $(B)^3\Pi(0_u^+)$," *Journal of Chemical Physics* 76: 5341-5349 (1982).

3. Clyne, M. A. A., M. C. Heaven and S. J. Davis. "Laser-Excitation Studies in Br_2," *Journal of the Chemical Society Faraday Transactions II* 76: 961-978 (1980).

4. Davis, S.J. "Potential of Halogen Molecules as Visible Chemical Laser Systems," AFWL-TR-79-104: 167, (1979).

5. Franck, J. "Elementary Processes of Photochemical Reactions," *Transactions of the Faraday Society* 21:536 (1925).

6. Herzberg, G. *Spectrum of Diatomic Molecules.* Van Nostrand, New York, 1953.

7. Hirschfelder, J.O., C.F. Curtis and R.B. Bird. *Molecular Theory of Gases and Liquids.* John Wiley and Sons, Inc., New York, 1110-1111, (1954).

8. Holmberg,C.D. Capt, USAF. *Spectroscopic and Vibrational Energy Transfer Studies in Molecular Bromine,* Doctoral Dissertation, Air Force Institute of Technology (AU), 1993.

9. Landau V. L. and E. Teller. *Phys Z Sovjetunion* 10: 34 (1936).

10. Melton, D. W. Capt, USAF. *Collisional Dynamics of the $B^3\Pi(0^+)$ State of BrF,* Doctoral Dissertation, Air Force Institute of Technology (AU), DS/ENP/91-01, August, 1991.

11. Montroll, E.W. and K.E. Shuler. "Studies in Nonequilibrium Rate Processes: The Relaxation of a System of Harmonic Oscillators," *Journal of Chemical Physics,* 26: 454 (1957).

12. Perram, G. P. Capt, USAF. *Collisional Dynamics of the B-State of Bromine Monochloride*, Doctoral Dissertation, Air Force Institute of Technology (AU), August, 1986.

13. Perram, G. P. and S. J. Davis. "Spectroscopic and Kinetic Studies of a Dye Laser Pumped $Br_2 B^3\Pi(0_u^+) \rightarrow X^1\Sigma_g^+$ Laser," *Journal of Chemical Physics* 84: 2526-2533 (1986).

14. Perram, G.P., D.W. Melton, T.L. Thompson and W.B. Roh. "Collisional Dynamics of the BrF $B^3\Pi(0^+)$ state. II. Vibrational Energy Transfer," *Journal of Chemical Physics*, 97(5) 3258-3264.

15. Schwartz, R.N., Z.I. Slawsky and K.F. Herzfeld. "Calculation of Vibrational Relaxation Times in Gases," *Journal of Chemical Physics*, 20: 1591 (1952).

16. Thompson, T.I. Capt, USAF. *Vibrational Energy Transfer in Bromine Monofluoride*, MS Thesis, Air Force Institute of Technology (AU), AFIT/GEP/ENP/91D-8, December, 1991.

17. Wolf, P. Capt, USAF. *Collisional Dynamics in the $B^3\Pi(0^+)$ State of Iodine Monofluoride*, Doctoral Dissertation, Air Force Institute of Technology (AU), 1986.

18. Wolf, P.J. and S.J. Davis. "Collisional Dynamics of the $IF(B)^3\Pi(0^+)$ State," *Journal of Chemical Physics*, 87(6): 3492 (1987).

19. Yardley, J.T. *Introduction to Molecular Energy Transfer*. Academic Press, New York, 95-110, (1980).

Appendix A.   Basic Energy Transfer Theories and Implementation[8]

This appendix describes the basic energy transfer processes used in this thesis. These include the gas kinetic collision rate,[12] the Schwartz, Slawsky and Herzfeld (SSH) theory,[15,19] and the Montroll-Shuler model.[11] The implementation of the Montroll-Shuler model as a user-defined function in Jandel-Scientific TableCurve is also presented as is a description of the five-level numerical solution to the Montroll-Shuler model with multi-quantum transfer.

Much of this Appendix is referenced from Holmberg[8] and is included here so that the serious reader will have the various references at his immediate disposal.

A.1   Gas Kinetic Collision Rates [8,12]

The elastic, hard sphere collision frequency for molecule A with collision partner B is given by

$$Z_A = N_B \, \sigma_g \, v_{AB} \qquad \qquad (A.1)$$

where

Z_A = collision frequency (sec^{-1})

N_B = particle B number density

σ_g = velocity - averaged collision cross section

   = $\pi (r_A + r_B)^2$

r_A, r_B = radius of particles A and B

v_{AB} = average relative speed = $(8k_BT/\pi\mu)^{1/2}$

μ = collision pair reduced mass

The rate constant for bimolecular gas kinetic collisions is given by

$$k_g = \sigma_g \, v_{AB} \qquad (A.2)$$

This value is commonly used as the standard for comparing the relative efficiency of various kinetic processes. The probability of occurrence for any given kinetic process is defined as

$$P = \sigma / \sigma_g \qquad (A.3)$$

where

   σ = cross-section for given kinetic process

   P = Probability for process σ occuring during a single collision

Hard sphere cross-sections, reduced masses, relative velocities and gas kinetic rate constants for Br_2 with the collision partners used in this study are given in Table A.1. Hard sphere cross sections were calculated with molecular radii derived for a (6,12) Lennard-Jones potential from viscosity data tabulated in reference (7).

Table A.1. Gas Kinetic Collision Parameters for Br_2 Collisions.

Buffer gas	Molecular diameter (Å)	Cross-section (Å²)	Reduced mass (a.u.)	Velocity (10^4cm/ sec)	Gas kinetic rate coefficient (10^{-10}cm³/ molec-sec)	Vibrational rate coefficient (10^{-11}cm³/ molec-sec)	Prob= k_v/k_g
N_2	3.681	49.63	23.79	5.76	2.86	3.37	0.118
NO	3.47	47.03	25.22	5.60	2.63	4.07	0.155
O_2	3.433	46.58	26.61	5.45	2.54	2.90	0.114
SF_6	5.51	75.09	75.89	3.23	2.42	3.19	0.131

A.2. SSH Theory.[8]

The SSH theory is another widely used vibrational transfer theory proposed by Schwartz, Slawsky and Herzfeld.[15] Often used as the basis for evaluating experimentally derived vibrational transfer rates, the SSH theory includes an attractive potential term that was neglected in the Landau-Teller Theory. Their potential has the form

$$V(r) = V_o \exp(-\alpha \cdot r) - \varepsilon \qquad (A.4)$$

The addition of the attractive term (ε = the potential well depth) causes a slight increase in translational energy just prior to reaching the repulsive potential, thus increasing vibrational transfer probabilities. The resulting probability for vibrational transfer from v'=1 to v'=0 for the SSH theory is given by Yardley [19] as

$$P_{10} \propto \left(\frac{\Theta'}{\Theta}\right)\left(\frac{\Theta'}{T}\right)^{1/6} \exp\left[-\frac{3}{2}(\Theta'/T)^{1/3} + (\Theta/2T) + (\varepsilon/k_B T)\right] \qquad (A.5)$$

where

$$\Theta' = 4\pi^2 L^2 \omega^2 \mu / k_B$$

$$\Theta = \hbar\omega / k_B$$

$$\hbar\omega = \text{vibrational energy}$$

$$L = \text{interaction length}$$

If the exponential terms dominate the probability function above, the logarithm of P_{10} can be written as

$$\ln(P_{10}) = A - B\, \mu^{1/3} \omega^{2/3} \qquad (A.6)$$

This form of the SSH vibrational transfer probability equation is most often used for examining experimentally determined vibrational transfer rate constants and cross-sections.

A.3 Montroll-Shuler Model TableCurve Implementation.[8]

An important analytical tool for this dissertation research was the TableCurve curve fitting software package from Jandel Scientific. The two TableCurve user-defined functions (UDF) allow the user to program customized functional forms to be used by the nonlinear least-squares fitting method. TableCurve also calculates a wide variety of statistical data for each fitting run.

For this study, it was necessary to implement the Montroll-Shuler solution to the master rate equation shown in the previous section as a user defined function UDF in TableCurve. The hypergeometric function,

$F\left(-v;-w;1;u^2\right)$ is not supported by TableCurve. The general form of the hypergeometric function is given as

$$F(a;b;c;x) = \sum_{n=0}^{\infty} \frac{(a)_n (b)_n}{(c)_n} \frac{x^n}{n!} \quad |x| < 1 \tag{A.7}$$

where $(a)_n$ is called a Pochhammer symbol given by

$$(a)_n = a(a+1)\cdots(a+n-1) \quad n = 1,2,3... \tag{A.8}$$

It is clear from Eqn A.15 that if a or b < 1, the hypergeometric series is finite. In other words, if $a = -m$, then $(-m)_n = 0$ for all $n \geq m$, thereby terminating the series. In the case of the Montroll-Shuler model, both a and b are negative and the hypergeometric function becomes

$$F\left(-v;-w;1;u^2\right) = \sum_{n=0}^{m} \frac{(-v)_n (-w)_n}{(1)_n} \frac{\left(u^2\right)^n}{n!} \tag{A.9}$$

where m is equal to the smaller value of v and w. TableCurve does not directly support the Pochhammer or hyperbolic sine functional forms, but the Pochhammer form can be written as

$$(-a)_n = (-1)^n a(a-1)(a-2)\cdots(a-n+1) = \frac{(-1)^n a!}{(a-n)!} \tag{A.10}$$

and the hyperbolic functions can be expressed as the difference of two exponential functions. The hypergeometric function can thus be simplified to the form

$$F\left(-v;-w;1;u^2\right) = v!w! \sum_{n=0}^{m} \frac{\left(u^2\right)^n}{(v-n)!(w-n)!(n!)^2} \tag{A.11}$$

The total general Montroll-Shuler function was implemented as a UDF in the following format:

$$T = 0.655$$

$$\#F1 = X\left[1 - \exp(-T)\right] \#A$$

$$\#F2 = \exp(-X/\#B)\left[1 - \exp(T)\right]\exp(w\,T)$$

$$\#F3 = \left[\exp(-\#F1) - 1\right]^{(v+w)}\Big/\left[\exp(-\#F1) - \exp(T)\right]^{(v+w+1)}$$

$$\#F4 = \left\{\left[\exp(T/2) - \exp(-T/2)\right]\Big/\left[\exp(\#F1/2) - \exp(-\#F1/2)\right]\right\}^2$$

$$\#F5 = (\#F4)^{n}\Big/\left\{(n!)^2(v-n)!(w-n)!\right\}$$

$$\#F6 = v!\,w!\sum_{n=0}^{m}\#F5$$

$$Y = \#C\;\#F2\;\#F3\;\#F6$$

where $T = \hbar\omega/k_B T$ is the ratio of the $Br_2(B)$ state vibrational energy spacing to the average thermal energy and #A, #B and #C are the fitting parameters where $\#A = \Gamma_v$, $\#B = 1/\Gamma_0$, and #C is a magnitude scaling factor.

The TableCurve model was tested for each pump/view level combination investigated by generating test data with Mathematica, which directly supports the hypergeometric function. In all cases, the curve fitting routine was able to exactly duplicate the test data inputs.

A.4 Development of the Eigenvalue Solution to a Five-level Montroll-Shuler System.[8]

This section discusses the methodology for obtaining the numerical eigenvalue solution for a five vibrational level system that follows Landau-Teller scaling and detailed balance. Landau-Teller scaling uses the vibrational transfer scaling rule $\Delta v = \pm 1$. Vibrational transfer rates are multiples of the fundamental vibrational transfer rate, $k_v(1,0)$, and scale as

$$k_{v \to v-1} = v \cdot k_v(1,0) \tag{A.12}$$

Inverse rates are calculated by detailed balance

$$k_{v \to v+1} = (v + 1) \cdot k_v(1,0) \exp(-\Delta E_{v+1,v}/kT) \qquad (A.13)$$

Additionally, it is assumed that the electronic removal rates are independent of vibrational level. These assumptions are identical to those of the Montroll-Shuler model with the exception of a finite number of vibrational levels. Therefore, Eq (A.12) can be used to calculate the rate matrix equation

$$\dot{z}(t) = \Gamma_v \begin{pmatrix} -\left(4 + 5e^{-\Theta}\right) & 4e^{-\Theta} & 0 & 0 & 0 \\ 4 & -\left(3 + 4e^{-\Theta}\right) & 3e^{-\Theta} & 0 & 0 \\ 0 & 3 & -\left(2 + 3e^{-\Theta}\right) & 2e^{-\Theta} & 0 \\ 0 & 0 & 2 & -\left(1 + 2e^{-\Theta}\right) & e^{-\Theta} \\ 0 & 0 & 0 & 1 & -e^{-\Theta} \end{pmatrix} z(t)$$

$$\qquad (A.14)$$

$$= Az(t) = \lambda z(t)$$

where

$$z(t) = x(t) \exp(\Gamma_o t)$$

$$\Theta = \Delta E_{v,v\pm1}/kT \approx .655$$

$$\Gamma_v = k_v(1,0)[M]$$

$$\Gamma_o = k_q[M] + 1/\tau_{rad}$$

Eigenvalues and eigenvectors were calculated for the rate matrix, **A** with Mathematica. Numerical solutions of the form

$$z_i(t) = \sum_j C_j u_i^j \exp(\lambda_j t) \qquad (A.15)$$

where

u_i^j is the ith element of the jth eigenvector

λ_j is the jth eigenvalue

and C_j are the initial condition constants defined by the equations

54

$$\mathbf{z}_i(0) = \sum_j C_j \mathbf{u}_i^j \qquad (A.16)$$

were written for each pump-view combination. Solutions were of the form

$$x_2(t) = D_1 \exp\{-(9.2\Gamma_v + \Gamma_o)t\} + D_2 \exp\{-(5.1\Gamma_v + \Gamma_o)t\}$$

$$+ D_3 \exp\{-(0.93\Gamma_v + \Gamma_o)t\} + D_4\{-(2.5\Gamma_v + \Gamma_o)t\} \qquad (A.17)$$

$$+ D_5 \exp\{-(0.04\Gamma_v + \Gamma_o)t\}$$

where the values for D_1 through D_5 were calculated from Eq (A.23). For the specific case of pump v'=3, view v'=2, the solution is

$$x_2(t) = -0.23 \exp\{-(9.2\Gamma_v + \Gamma_o)t\} - 0.28 \exp\{-(5.1\Gamma_v + \Gamma_o)t\}$$

$$+ 0.3370 \exp\{-(0.93\Gamma_v + \Gamma_o)t\} + 0.088\{-(2.5\Gamma_v + \Gamma_o)t\}$$

$$+ 0.084 \exp\{-(0.04\Gamma_v + \Gamma_o)t\}$$

The relative magnitudes of the coefficients may determine if one of the five exponential terms will dominate the temporal profile of the simulated data.

A.5 Development of the Eigenvalue Solution to a Five-level Montroll-Shuler System with Multi-Quantum Transfer.[8]

The development of the eigenvalue solution for the five-level vibrational transfer model with multi-quantum effects is identical to that described in the previous section except that non-zero multi-quantum transfer rates have been included in the $\Delta v = \pm 2$ off diagonal elements of the vibrational transfer rate matrix. It is reasonable to assume that the multi-quantum transfer rate coefficients are proportional to the rate coefficients for single-quantum transfer from the same vibrational level. For the current

development, the multi-quantum elements were scaled according to the relationship

$$
\begin{aligned}
k_{v \to v-2} &= f \cdot k_{v \to v-1} \\
&= f \cdot v \cdot k_v(1,0)
\end{aligned}
\tag{A.18}
$$

where f is a number less than unity and inverse rates are determined by detailed balance as in Eq (A.20). The rate matrix, $\mathbf{A}$, in Eq(A.21) becomes

$$
\Gamma_v
\begin{pmatrix}
-\left(\begin{array}{c}4+5e^{-\Theta}\\+4f+6fe^{-2\Theta}\end{array}\right) & 4e^{-\Theta} & 4fe^{-2\Theta} & 0 & 0 \\[2em]
4 & -\left(\begin{array}{c}3+4e^{-\Theta}\\+3f+5fe^{-2\Theta}\end{array}\right) & 3e^{-\Theta} & 3fe^{-2\Theta} & 0 \\[2em]
4f & 3 & -\left(\begin{array}{c}2+3e^{-\Theta}\\+2f+4fe^{-2\Theta}\end{array}\right) & 2e^{-\Theta} & 2fe^{-2\Theta} \\[2em]
0 & 3f & 2 & -\left(\begin{array}{c}1+2e^{-\Theta}\\+3fe^{-2\Theta}\end{array}\right) & e^{-\Theta} \\[2em]
0 & 0 & 2f & 1 & -\left(\begin{array}{c}e^{-\Theta}\\+2fe^{-2\Theta}\end{array}\right)
\end{pmatrix}
$$

For the pump v'=3, view v'=2 condition with f=0.2, the five exponential eigenvalue solution for $x_2(t)$ is given by

$$
x_2(t) = D_1 \exp\left\{-(10.0\Gamma_v + \Gamma_o)t\right\} + D_2 \exp\left\{-(6.1\Gamma_v + \Gamma_o)t\right\}
$$

$$
+ D_3 \exp\left\{-(1.3\Gamma_v + \Gamma_o)t\right\} + D_4\left\{-(3.2\Gamma_v + \Gamma_o)t\right\}
\tag{A.19}
$$

$$
+ D_5 \exp\left\{-(0.06\Gamma_v + \Gamma_o)t\right\}
$$

where the coefficients are calculated from Eq (A.23) as before.

Appendix B.   Spectral Overlap and Systematic Error

B.1   Spectral Overlap

At the monochromator resolution of 22.4 Å,[10] the odd numbered v'
levels do not significantly overlap the even numbered v' levels, however, the
overlaps between odd only or even only v' transitions are considerable.[8] The
overlap fractions for the (v',v") transitions in Table B.1 were determined by
Holmberg from comparisons of the Franck-Condon factor of the (v',v")
transition and the Franck-Condon factors of the (v'±2, v"±1) transitions.

Table B.1. Spectral overlap fractions and observation wavelengths [8].

Observed transition (v',v")	v'=	0	1	2	3	4	Monochromator Wavelength (Angstroms)
(1,12)		.00	.97	.00	.03	.00	8162
(2,11)		.09	.00	.90	.00	.01	7860
(3,9)		.00	.13	.00	.87	.00	7425

B.2   Calibration

The experiment used the same components as Holmberg's experiments[8],
and the calibrations of the monochromator and dye laser were accomplished by
him.

B.3 Statistical Errors

The Stern-Volmer plots were analyzed by linear regression, and the error for the rate coefficient was the standard deviation. The average rate coefficients listed in Tables 4, 5, and 6 for each individual pump/view level are a weighted average of the slopes. The error listed for the rate coefficients is the standard deviation from this average divided by $1/\sqrt{(N-2)}$ where N is the number of measurements made.

The sources of error in the coefficients are due to three main factors. The first is assuming that the vibrationally resolved profiles are free from overlap from other vibrational levels. Because of the Franck-Condon factors, the overlap should be small, and the largest percentage of overlap consisted of 13% from Table B.1.

The second source of error is in the assignment of a t = 0 reference time to the individual waveforms. This was done when fitting the waveform in TableCurve. Two different methods were tested and differed by less than 10%.

The third source of error was a relatively low signal to noise ratio of five compared to Holmberg's lowest SNR of ten.[8] Considering these three errors, the systematic error for the rate coefficients is estimated to be less than 30%, which is fairly good considering the low signal to noise ratios encountered.

Appendix C. Molecular Buffer Gas Vibrational Transfer Data

This appendix includes plots of the vibrational transfer data from the buffer gas studies discussed in Chapter IV. Vibrational transfer waveforms and the respective Montroll-Shuler fits as well as typical Stern-Volmer plots used to derive the fundamental vibrational transfer rate coefficents and quenching rates are included for each collision parter. Additionally, logarithmic displays of the Montroll-Shuler fits to satellite waveforms are presented to emphasize non-Montroll-Shuler behavior, especially at higher pressures.
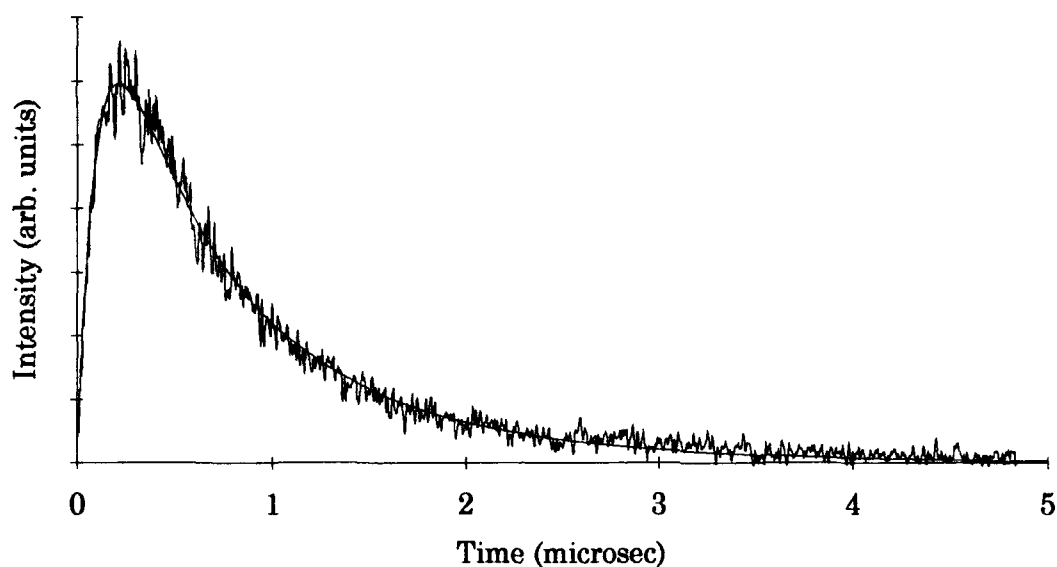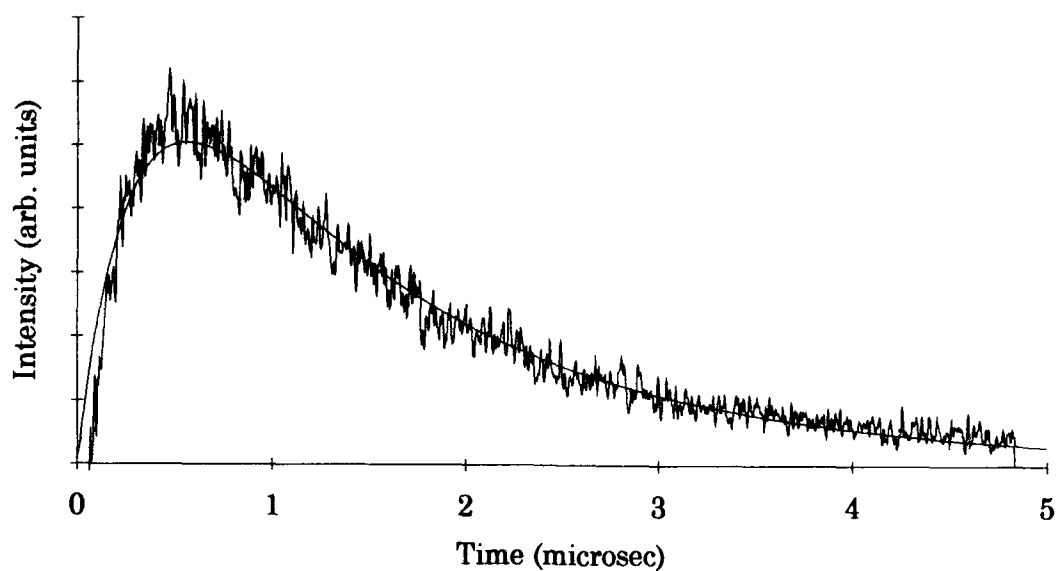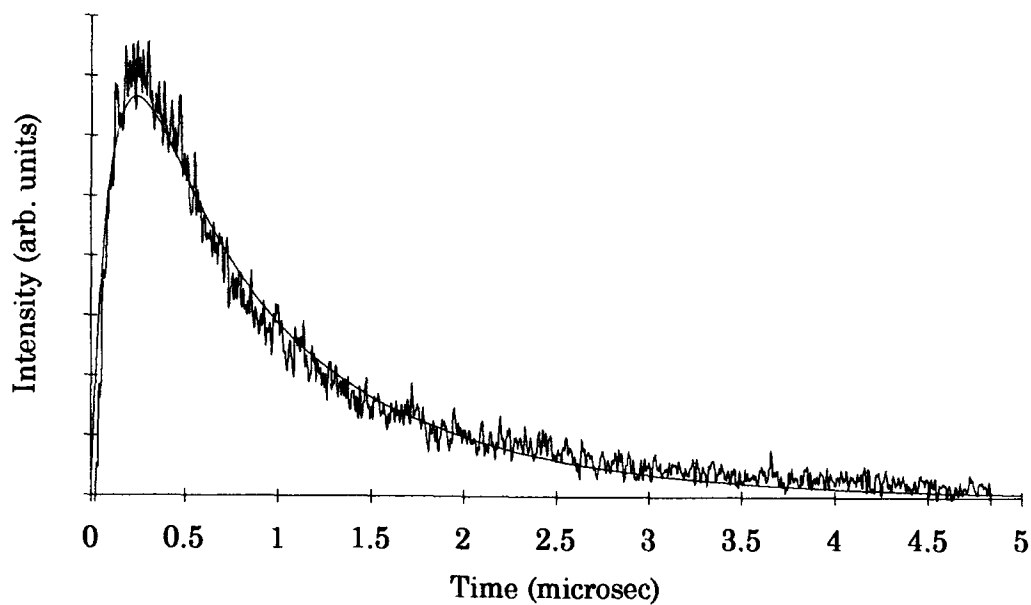
Figure C.1. Montroll-Shuler fit to emissions from the pump v'=3, view v'=2 (p3v2), with a Br_2 pressure of 704 mTorr and O_2 pressure of 226 mTorr.
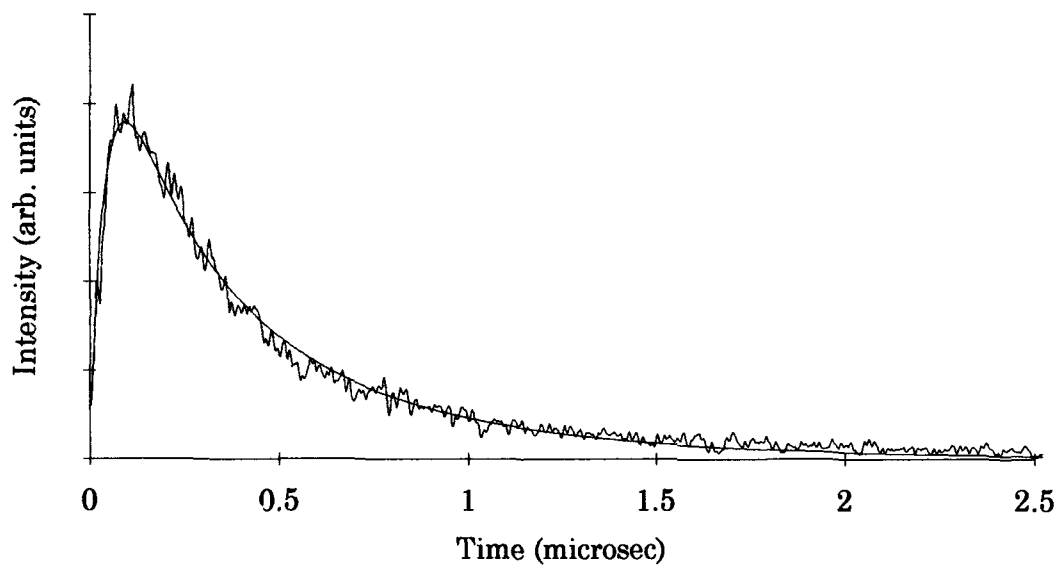
Figure C.2. Montroll-Shuler fit to emissions from the pump v'=3, view v'=2 (p3v2), with a Br_2 pressure of 704 mTorr and O_2 pressure of 1940 mTorr.
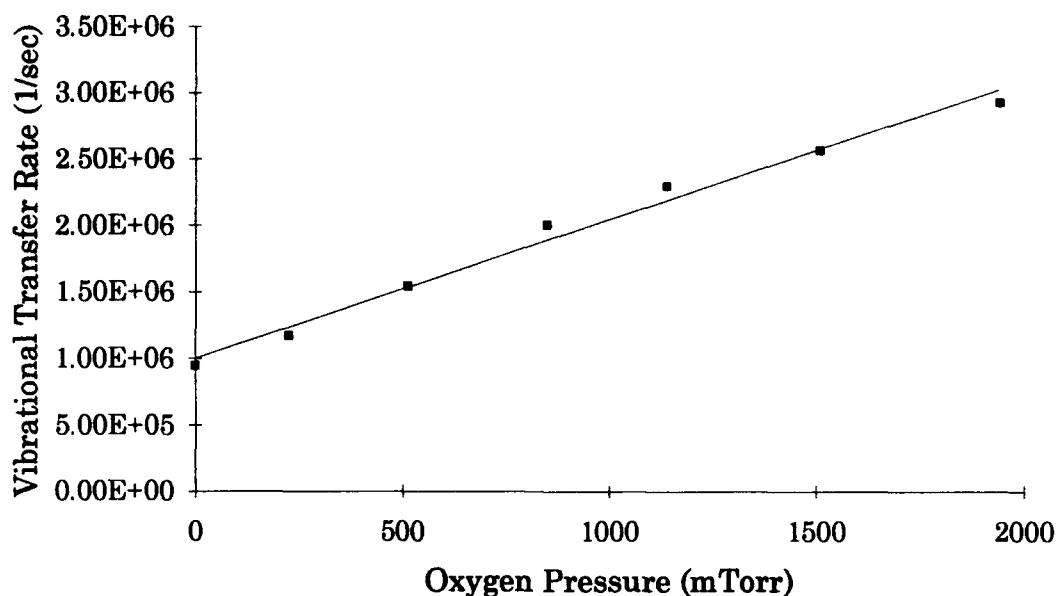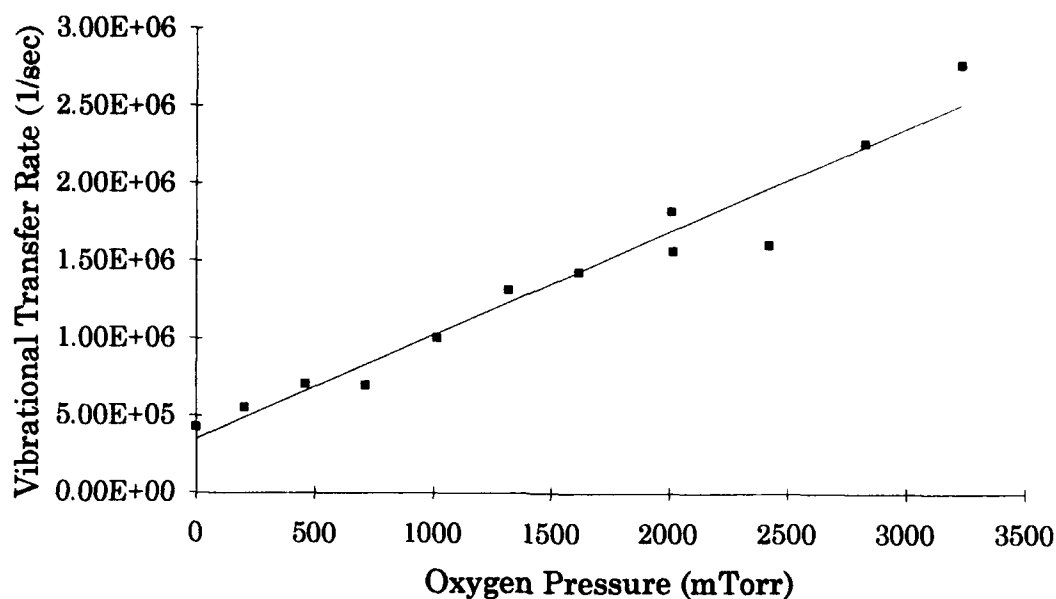
Figure C.3. Stern-Volmer plot of the Montroll-Shuler vibrational transfer fits to pump v'=3, view v'=2 of 704 mTorr Br_2 with O_2 buffer gas that gives $k_v(1,0)$=3.8 ($\pm$0.2) x 10^{-11} cm^3/molec-sec.
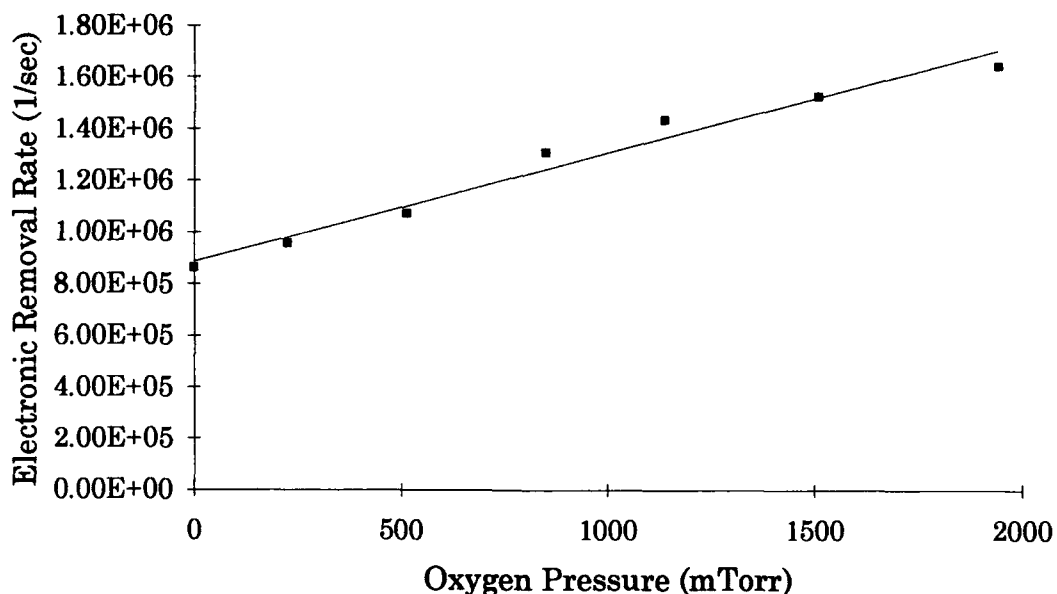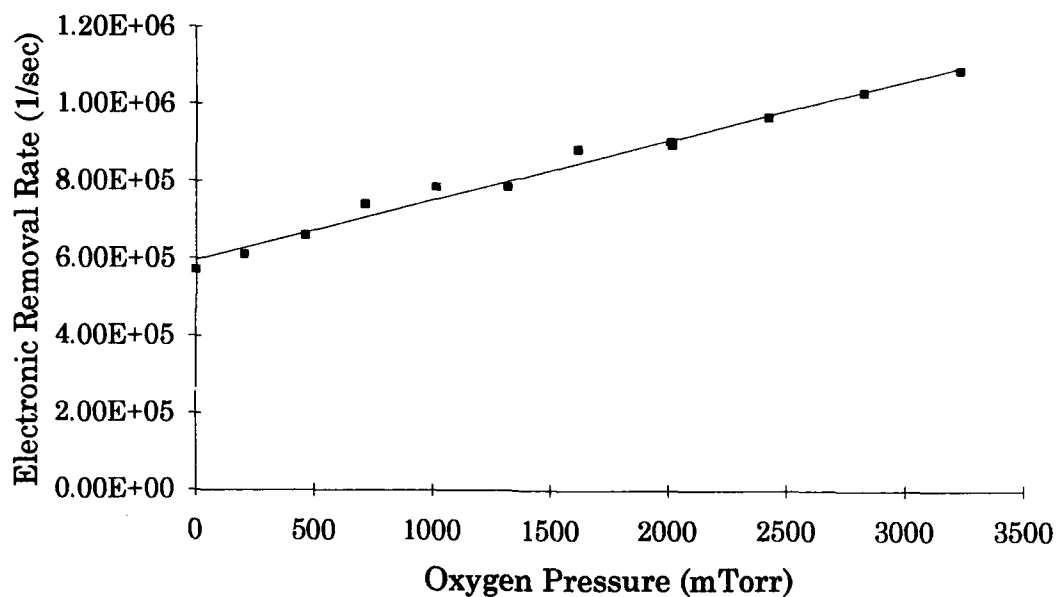

Figure C.4. Stern-Volmer plot of the Montroll-Shuler electronic quenching fits to pump v'=3, view v'=2 of 704 mTorr Br_2 with O_2 buffer gas that gives k_q=1.6 ($\pm$0.2) x 10^{-11} cm^3/molec-sec.
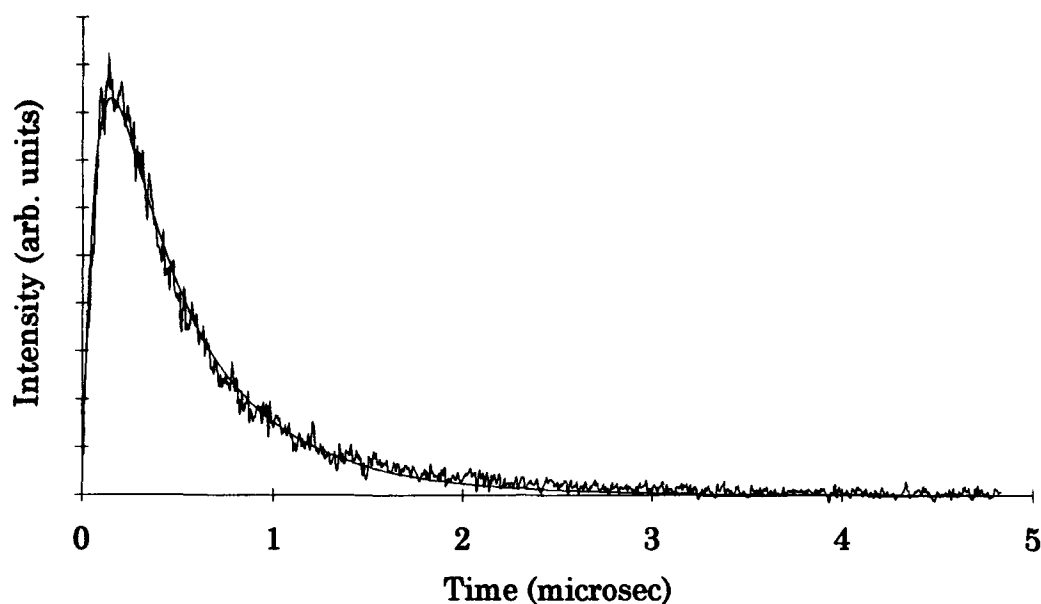
Figure C.5. Montroll-Shuler fit to emissions from the pump v'=2, view v'=3
(p2v3), with a Br_2 pressure of 568 mTorr and O_2 pressure of
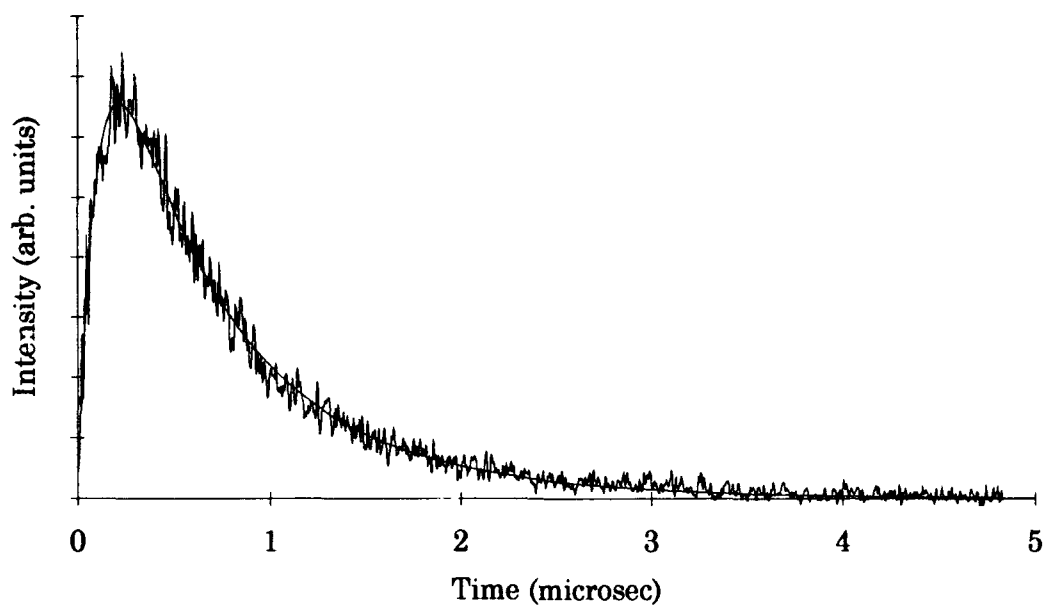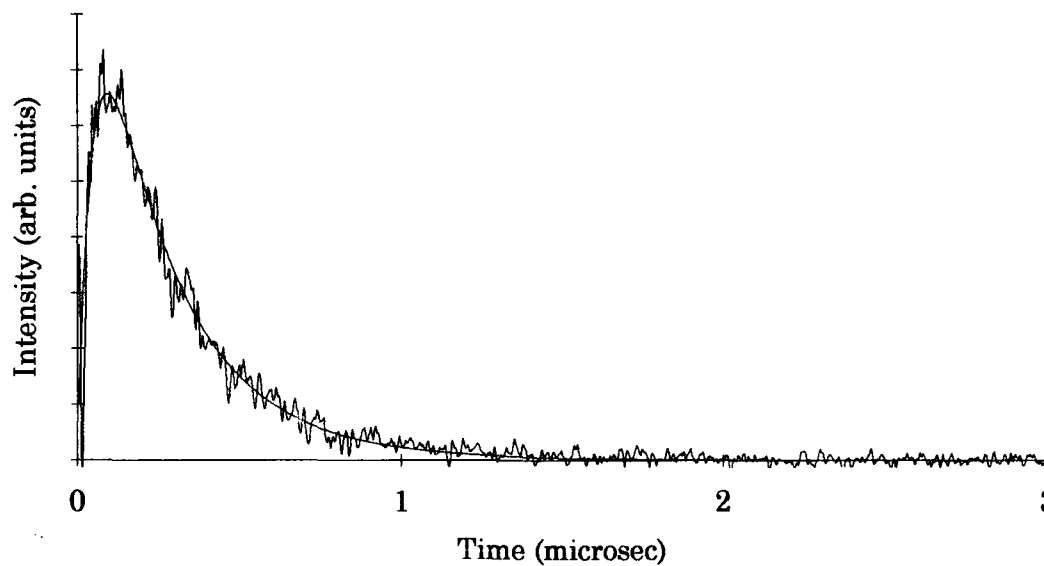227 mTorr.
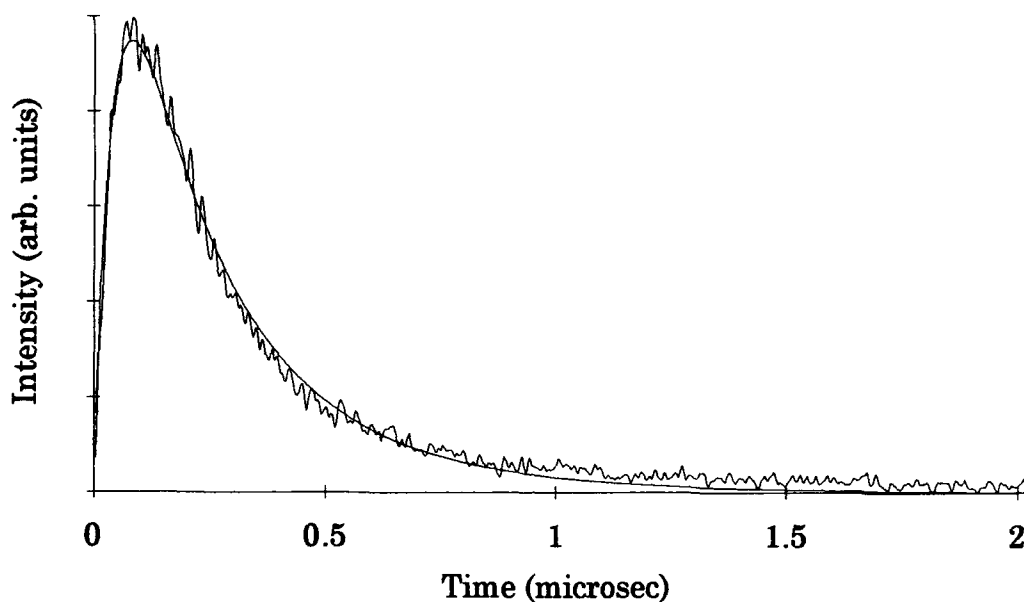
Figure C.6. Montroll-Shuler fit to emissions from the pump v'=2, view v'=3
(p2v3), with a Br_2 pressure of 568 mTorr and O_2 pressure of
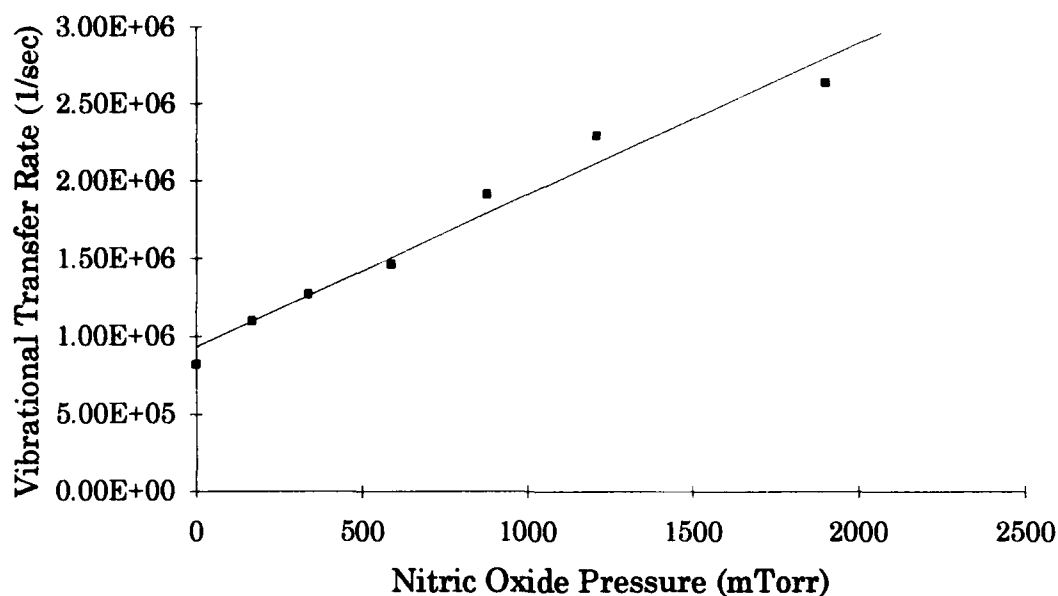2181 mTorr.
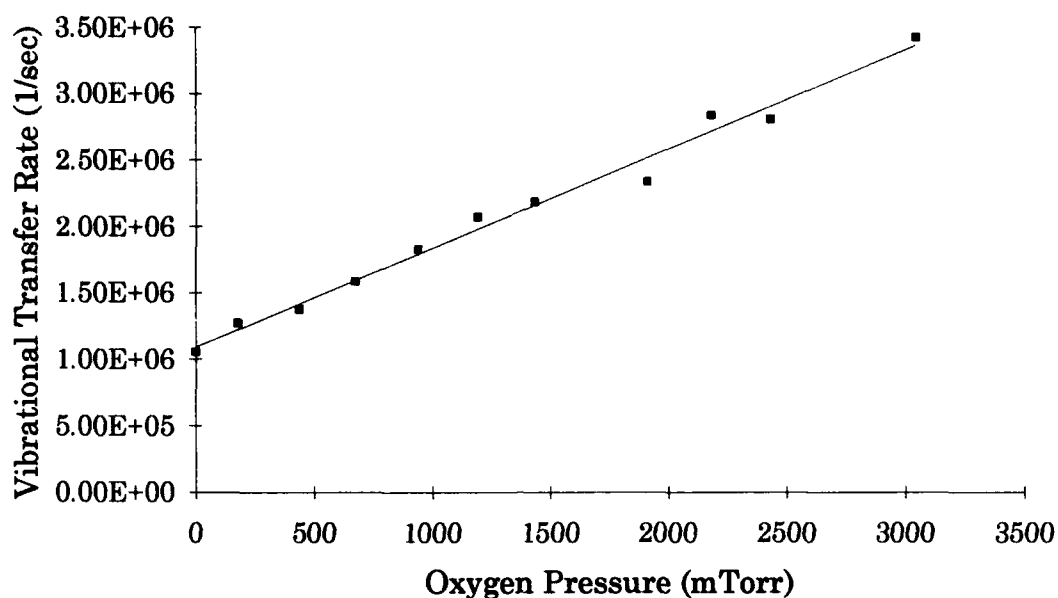
Figure C.7. Stern-Volmer plot of the Montroll-Shuler vibrational transfer fits
to pump v'=2, view v'=3 of 568 mTorr Br_2 with O_2 buffer gas that
gives $k_v(1,0)$=2.7 ($\pm$0.1) x 10^{-11} cm^3/molec-sec.
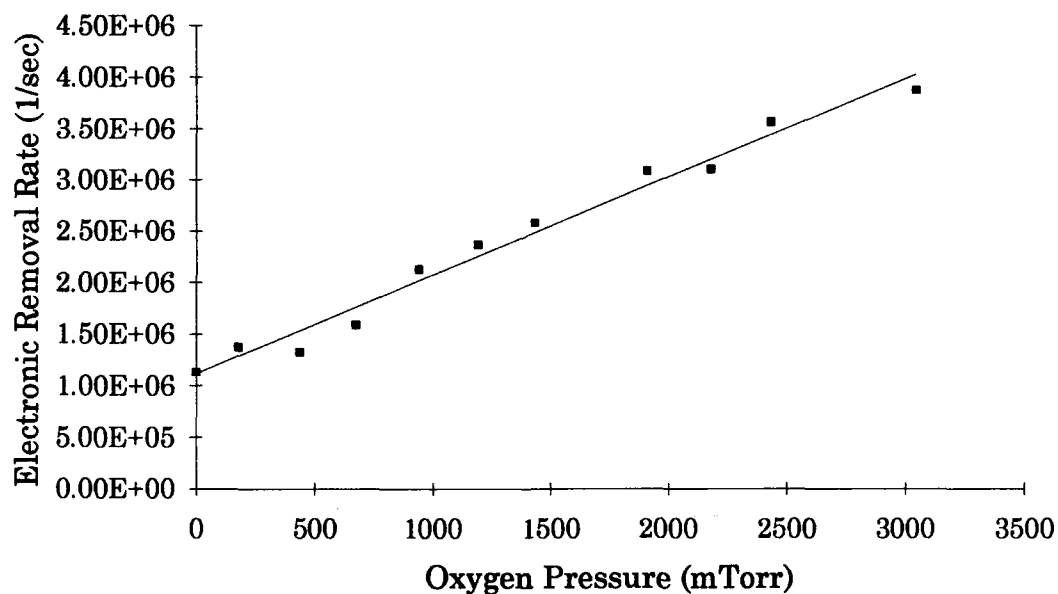
Figure C.8. Stern-Volmer plot of the Montroll-Shuler electronic quenching
fits to pump v'=2, view v'=3 of 568 mTorr Br_2 with O_2 buffer gas
that gives k_q=3.5 ($\pm$0.2) x 10^{-11} cm^3/molec-sec.

Figure C.9. Montroll-Shuler fit to emissions from the pump v'=2, view v'=1 (p2v1), with a Br_2 pressure of 586 mTorr and O_2 pressure of 203 mTorr.

Figure C.10. Montroll-Shuler fit to emissions from the pump v'=2, view v'=1 (p2v1), with a Br_2 pressure of 586 mTorr and O_2 pressure of 2423 mTorr.

64

Figure C.11. Stern-Volmer plot of the Montroll-Shuler vibrational transfer fits to pump v'=2, view v'=1 of 586 mTorr Br_2 with O_2 buffer gas that gives $k_v(1,0)=2.5$ (± 0.2) x 10^{-11} cm^3/molec-sec.
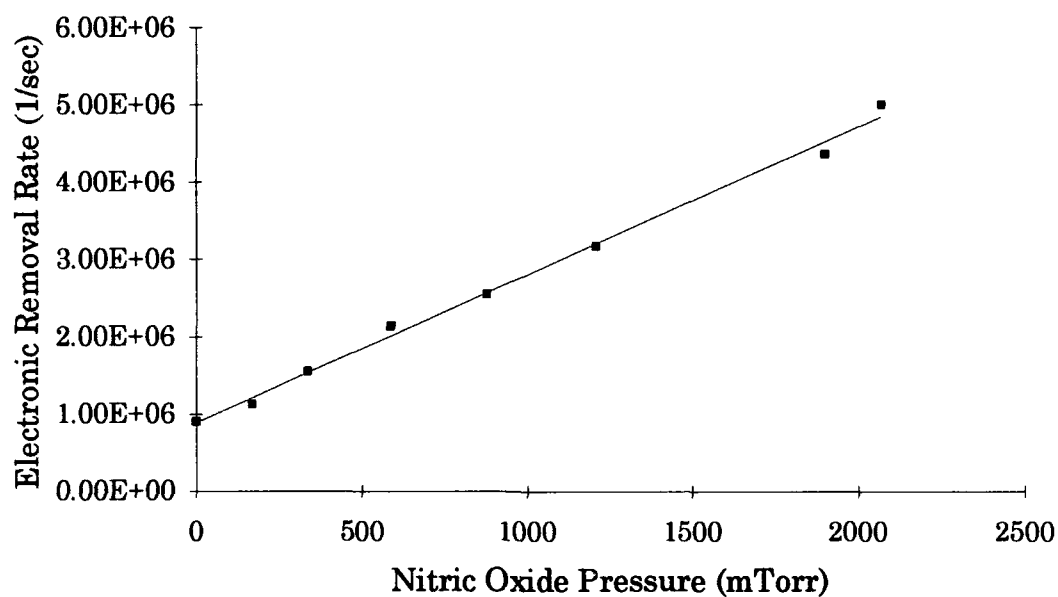

Figure C.12. Stern-Volmer plot of the Montroll-Shuler electronic quenching fits to pump v'=2, view v'=1 of 586 mTorr Br_2 with O_2 buffer gas that gives $k_q=0.57(\pm 0.02)$ x 10^{-11} cm^3/molec-sec.
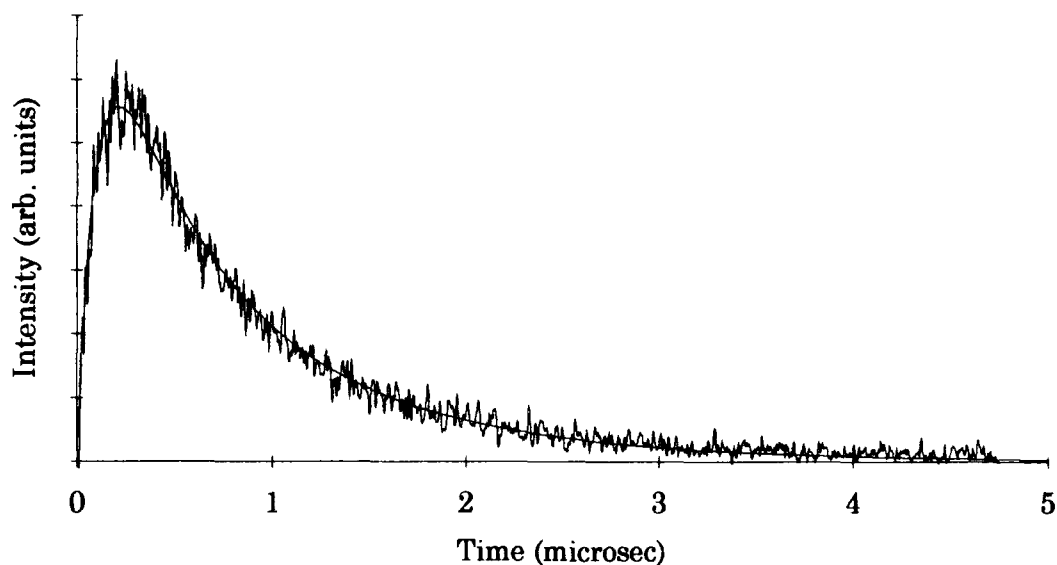
Figure C.13. Montroll-Shuler fit to emissions from the pump v'=3, view v'=2
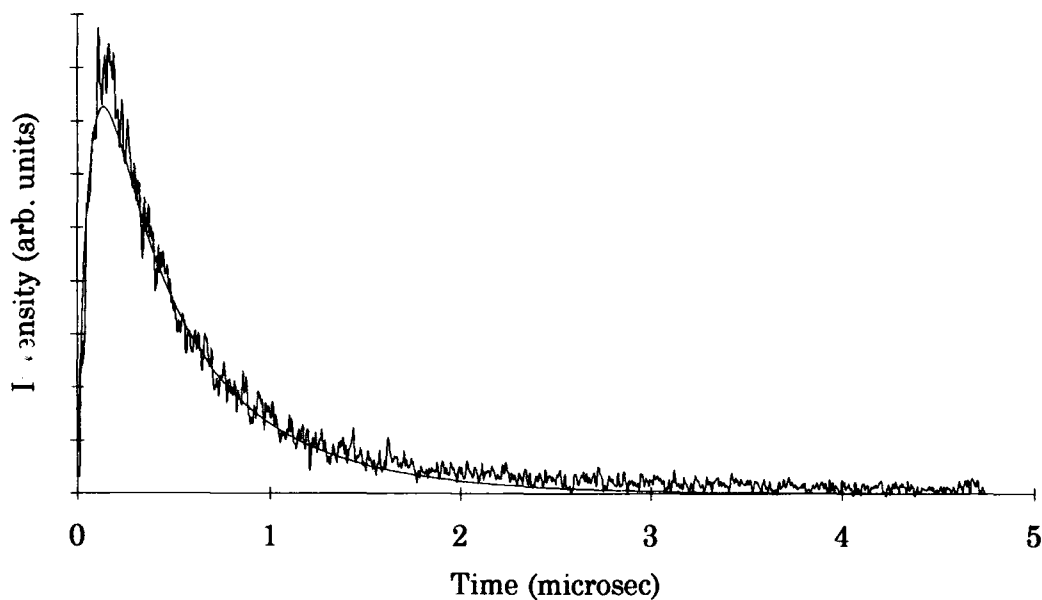(p3v2), with a Br_2 pressure of 659 mTorr and NO pressure of 168
mTorr.

Figure C.14. Montroll-Shuler fit to emissions from the pump v'=3, view v'=2
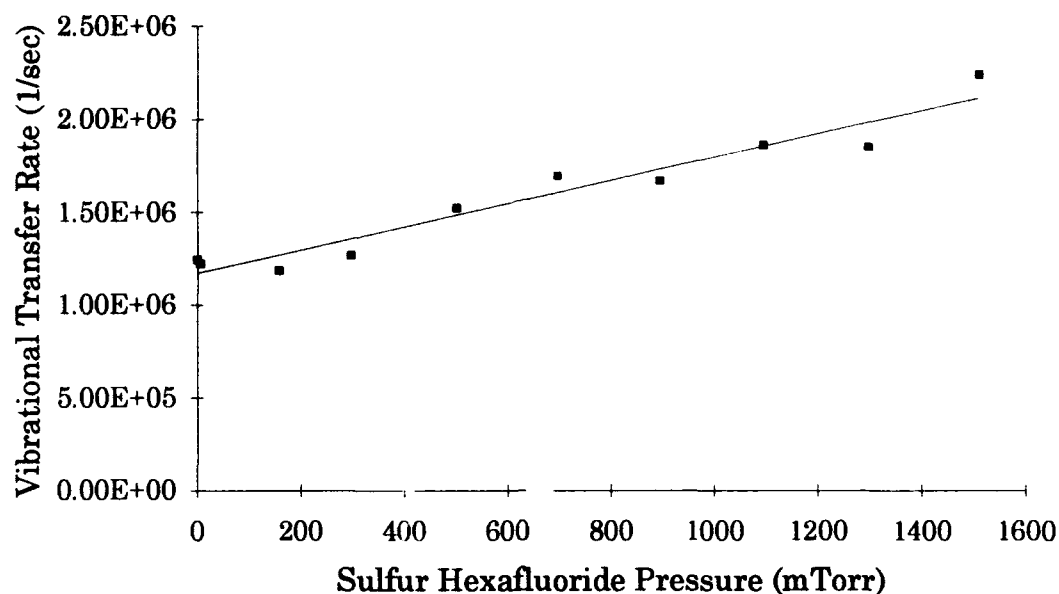(p3v2), with a Br_2 pressure of 659 mTorr and NO pressure of 1208
mTorr.

Figure C.15. Stern-Volmer plot of the Montroll-Shuler vibrational transfer fits to pump v'=3, view v'=2 of 659 mTorr Br_2 with NO buffer gas that gives $k_v(1,0)$=3.6 ($\pm$0.3) x 10^{-11} cm^3/molec-sec.
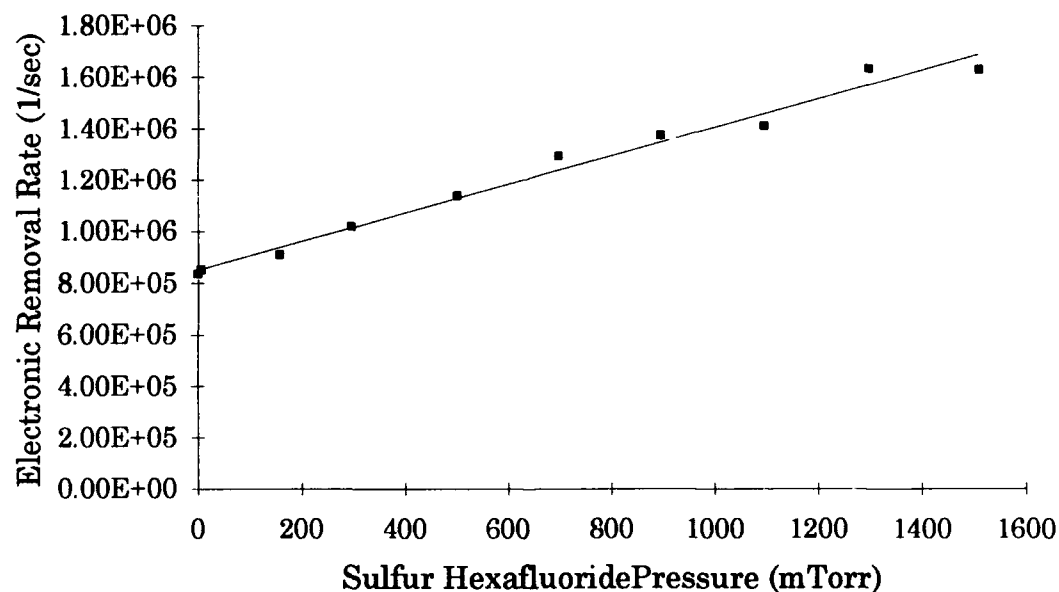

Figure C.16. Stern-Volmer plot of the Montroll-Shuler electronic quenching fits to pump v'=3, view v'=2 of 659 mTorr Br_2 with NO buffer gas that gives k_q=7.1($\pm$0.2) x 10^{-11} cm^3/molec-sec.

Figure C.17. Montroll-Shuler fit to emissions from the pump v'=3, view v'=2 (p3v2), with a Br_2 pressure of 708 mTorr and SF_6 pressure of 157mTorr.

Figure C.18. Montroll-Shuler fit to emissions from the pump v'=3, view v'=2 (p3v2), with a Br_2 pressure of 708 mTorr and SF_6 pressure of 1094 mTorr.

Figure C.19. Stern-Volmer plot of the Montroll-Shuler vibrational transfer fits to pump v'=3, view v'=2 of 708 mTorr Br_2 with SF_6 buffer gas that gives $k_v(1,0)=2.3(\pm0.2) \times 10^{-11}$ cm^3/molec-sec.

Figure C.20. Stern-Volmer plot of the Montroll-Shuler electronic quenching fits to pump v'=3, view v'=2 of 708 mTorr Br_2 with SF_6 buffer gas that gives $k_q=2.1(\pm0.1) \times 10^{-11}$ cm^3/molec-sec.
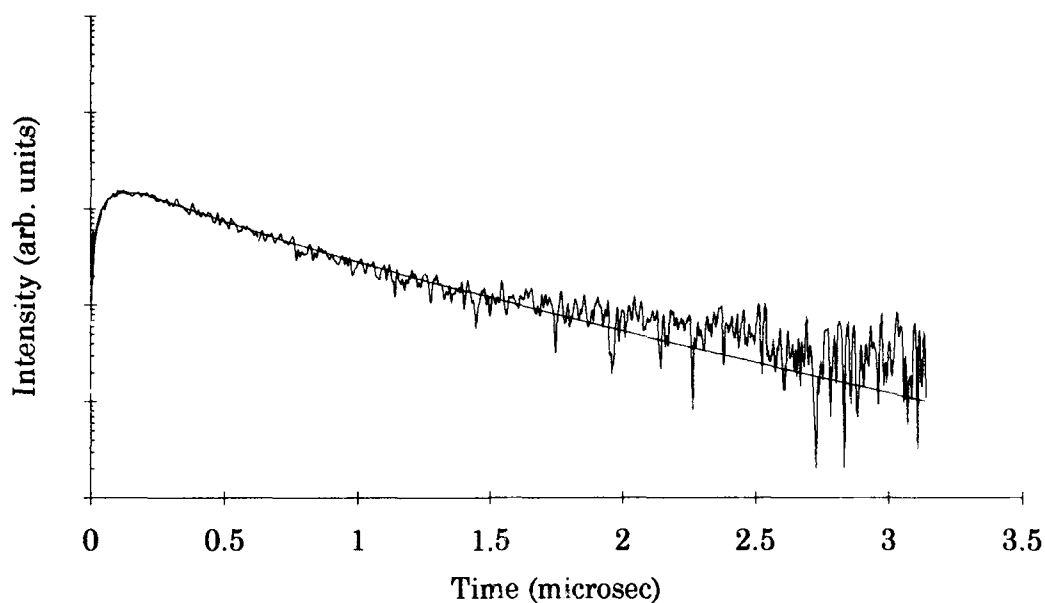
Figure C.21. Logarithmic Montroll-Shuler fit to emissions from the pump
v'=3, view v'=2 (p3v2), with a Br_2 pressure of 802 mTorr and N_2
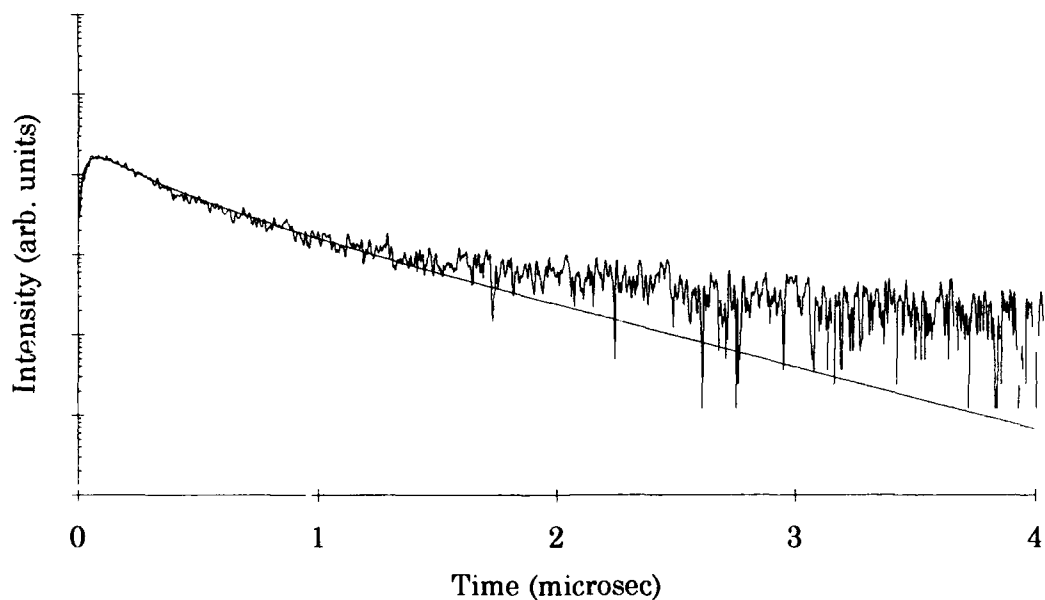pressure of 788 mTorr.

Figure C.22. Logarithmic Montroll-Shuler fit to emissions from the pump
v'=3, view v'=2 (p3v2), with a Br_2 pressure of 802 mTorr and N_2
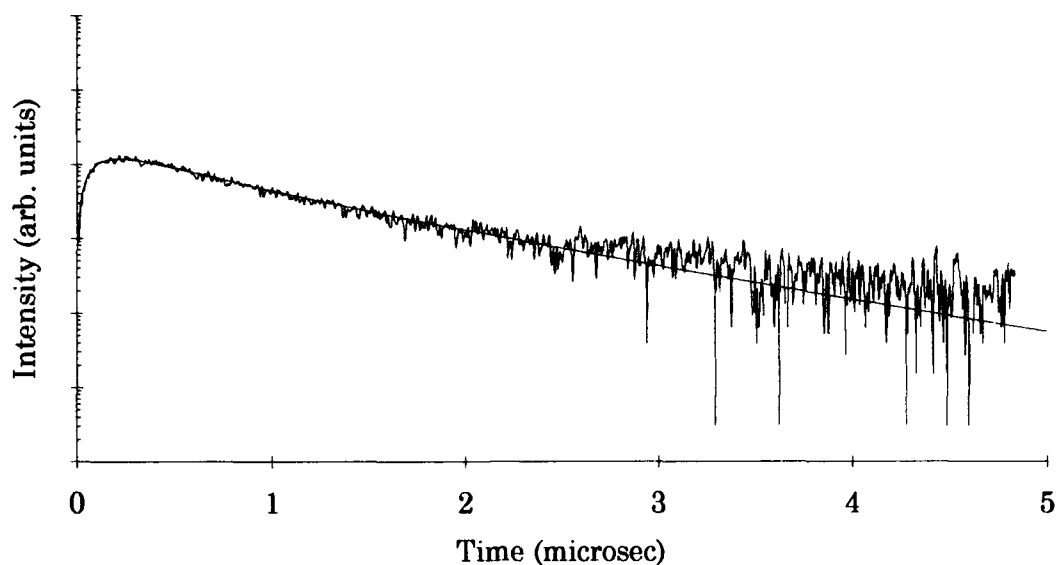pressure of 2397 mTorr

Figure C.23. Logarithmic Montroll-Shuler fit to emissions from the pump
v'=3, view v'=2 (p3v2), with a Br_2 pressure of 704 mTorr and O_2
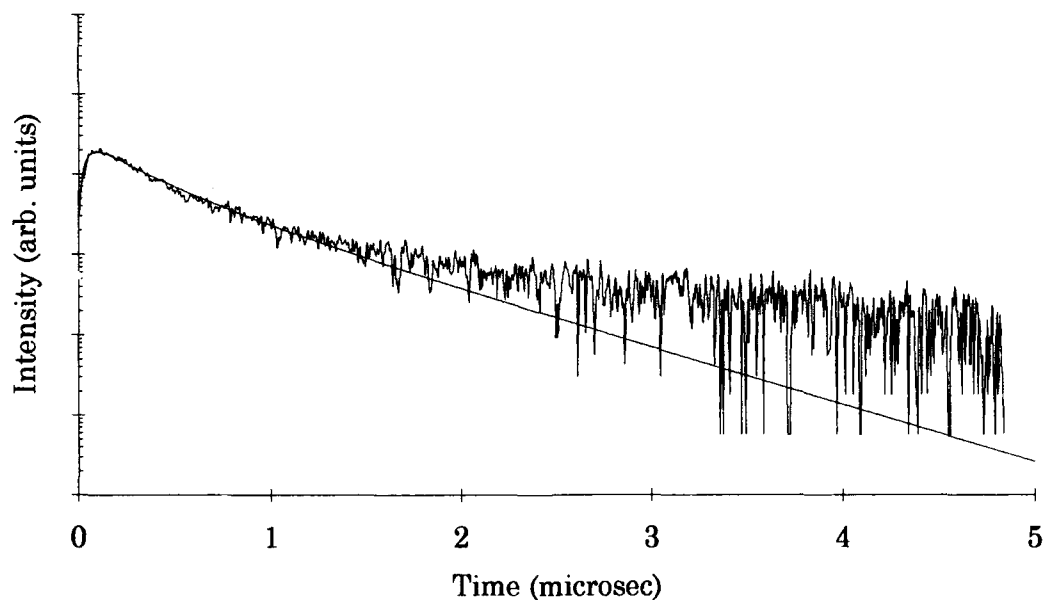pressure of 226 mTorr.

Figure C.24. Logarithmic Montroll-Shuler fit to emissions from the pump
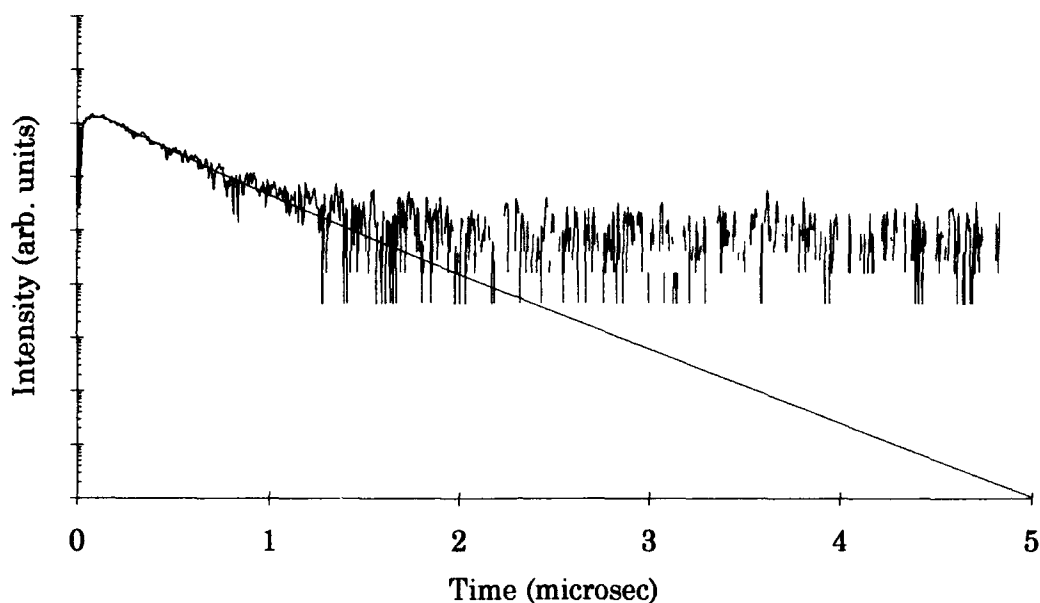v'=3, view v'=2 (p3v2), with a Br_2 pressure of 704 mTorr and O_2
pressure of 1940 mTorr.

Figure C.25. Logarithmic Montroll-Shuler fit to emissions from the pump v'=3, view v'=2 (p3v2), with a Br_2 pressure of 659 mTorr and NO pressure of 1208 mTorr.
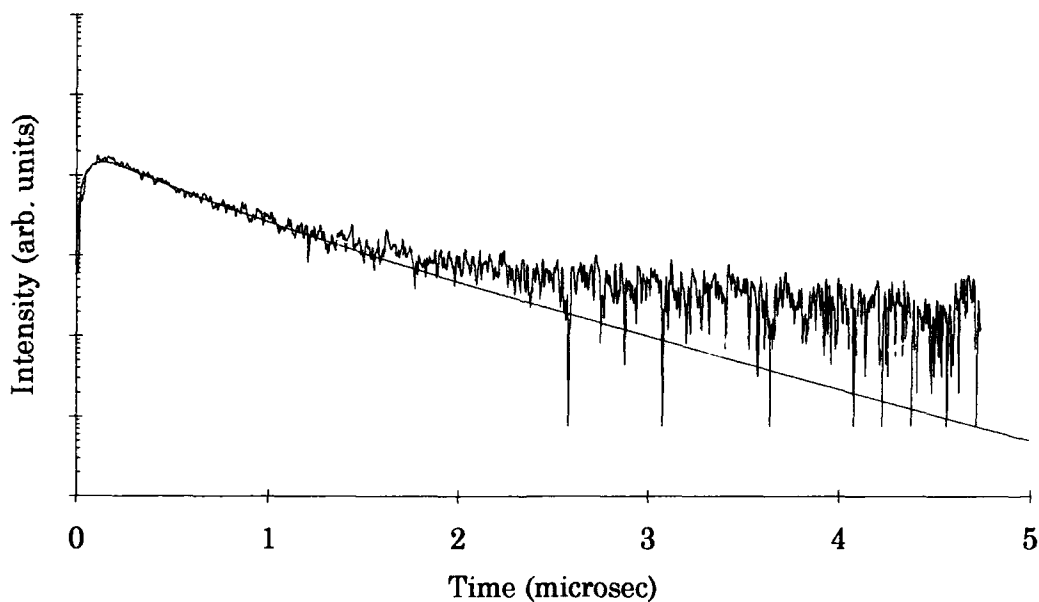

Figure C.26. Logarithmic Montroll-Shuler fit to emissions from the pump v'=3, view v'=2 (p3v2), with a Br_2 pressure of 708 mTorr and SF_6 pressure of 1094 mTorr.

Vita

Captain Gregory S. Williams was born on June 27, 1966, in Fort Walton Beach, Florida. He graduated from Fort Walton Beach High School in 1984 and then attended the United States Naval Academy from which he received the degree of Bachelor of Science in Physics, with distinction, in May 1988. Upon graduation, he received a commission as a Second Lieutenant in the USAF and entered Undergraduate Navigator Training at Mather AFB, California in August 1989. After receiving his aeronautical rating as a Navigator and Electronic Warfare Officer in October 1989, he continued his training in the AT-38B at Holloman AFB, New Mexico, the F-4E at George AFB, California, and the RF-4C at Boise ANGB, Idaho. He was assigned to the 12th Tactical Reconnaissance Squadron, Bergstrom AFB, Texas as a Weapons Systems Officer until he entered AFIT in May 1992.

Greg married Margaret Harsany of Eagleville, Pennsylvania in 1990, and is currently assigned to the 561st Fighter Squadron, Nellis AFB, Nevada.

Permanent Address: 106 Memorial Pkwy
Fort Walton Beach, FL 32548

1. AGENCY USE ONLY (Leave blank)	2. REPORT DATE December 1993	3. REPORT TYPE AND DATES COVERED Master's Thesis

4. TITLE AND SUBTITLE

Vibrational Energy Transfer Within The $B^3\Pi(O_u)$ State Of $^{79}Br_2$ Upon Collision With N_2, O_2, NO, And SF_6

5. FUNDING NUMBERS

6. AUTHOR(S)

Gregory S. Williams, Captain, USAF

7. PERFORMING ORGANIZATION NAME(S) AND ADDRESS(ES)

Air Force Institute of Technology, WPAFB OH 45433-6583

8. PERFORMING ORGANIZATION REPORT NUMBER

AFIT/GAP/ENP/93D-10

9. SPONSORING/MONITORING AGENCY NAME(S) AND ADDRESS(ES)

Dr. Ernie Dorko
PL/LID
Kirtland AFB, NM 87117-6008

10. SPONSORING/MONITORING AGENCY REPORT NUMBER

11. SUPPLEMENTARY NOTES

12a. DISTRIBUTION/AVAILABILITY STATEMENT

Approved for public release; distribution unlimited

12b. DISTRIBUTION CODE

13. ABSTRACT (Maximum 200 words)

Vibrational transfer and electronic quenching in the lower vibrational levels of the $^{79}Br_2$(B; $v'\leq3$) were investigated using spectrally resolved, temporally resolved pulsed laser induced fluorescence techniques. Spectrally resolved emissions from collisionally populated Br_2(B) vibrational levels were observed for N_2, O_2, NO, and SF_6 collision partners. The vibrational transfer was efficient in the nonpredissociatve vibrational levels and is adequately described by the Montroll-Shuler model. An average fundamental vibrational transfer rate coefficient of $k_v(1,0)=3.4(\pm0.6)\times10^{-11}cm^3$/molec-sec predicts the vibrational transfer rates for the $0\leq v'\leq3$ collisions with N_2, and a rate of $k_v(1,0)=2.9(\pm0.6)\times10^{-11}cm^3$/molec-sec for collisions with O_2. Vibrational rates for NO and SF_6 range from $1.5(\pm0.2)\times10^{-11}cm^3$/molec-sec to $4.0(\pm1.1)\times10^{-11}cm^3$/molec-sec. Electronic quenching rates for the observed vibrational levels were determined from the same data. Quenching rates were seen to be vibrationally dependent and went from a low of $k_q=0.4(\pm0.1)\times10^{-11}cm^3$molec-sec for N_2 (pump $v'=2$, view $v'=1$) to a high of $k_q=6.9(\pm1.1)\times10^{-11}cm^3$/molec-sec for NO (pump $v'=3$, view $v'=2$).

14. SUBJECT TERMS

Bromine, interhalogens, vibrational energy transfer, laser induced fluorescence, rate coefficient, molecular gases, Montroll-Shuler model

15. NUMBER OF PAGES 73

16. PRICE CODE

17. SECURITY CLASSIFICATION OF REPORT Unclassified	18. SECURITY CLASSIFICATION OF THIS PAGE Unclassified	19. SECURITY CLASSIFICATION OF ABSTRACT Unclassified	20. LIMITATION OF ABSTRACT UL